TAMPEREEN TEKNILLINEN YLIOPISTO
TAMPERE UNIVERSITY OF TECHNOLOGY

EMMI VÄLIMÄKI

MODELLING, SIMULATION AND VALIDATION OF CMT PROCESS: AN APPLICATION FOR ADDITIVE MANUFACTURING

Master of Science thesis

Examiners: Prof. Eric Coatanéa and Prof. Petri Vuoristo. Examiners and topic approved by the Faculty Council of Engineering Sciences on 7th of September 2016

ABSTRACT

EMMI VÄLIMÄKI: MODELLING, SIMULATION AND VALIDATION OF CMT PROCESS: AN APPLICATION FOR ADDITIVE MANUFACTURING
Tampere University of Technology
Master of Science Thesis, 63 pages.
February 2017
Master's Degree Programme in Material Engineering
Major: Metal materials
Examiners: Professor Eric Coatanea and Professor Petri Vuoristo

Keywords: Additive manufacturing, modelling, DACM, Cold Metal Transfer, DED, AlSi5, 316L

Traditional welding, among the many other processes has been given promise to the additive manufacturing industries. Creating models to predict the quality of the manufactured part can be highly beneficial and can create useful knowledge of the process and material. In this thesis, a cold metal transfer (CMT) technology was modelled for single bead using dimensional analysis conceptual modelling (DACM). DACM is a method that supports the production of model. The method can be used different ways and in this thesis, two of the ways are presented, with the use of already known theory and without the knowledge. Method uses several different modelling methods, such as dimensional analysis, bond graph theory and causality rules.

CMT technology is an arc welding method. It differs from the typical welding method in such a way that the wire feed pulls in causing the droplet to detach. This movement can happen between 50-130 Hz and it reduces the heat input to the substrate material. Since the CMT is a highly-controlled system it has some parameters that are not know by user. These parameters were clarified during this thesis. Simple regression model was created to understand how the parameters affect. Materials in use was aluminium alloy AlSi5 and stainless steel 316L.

Creation of the regression model was carried out with Taguchi design of experiments (DoE). Results were analysed by analysis of variance (ANOVA) and a nonlinear regression was created to understand how CMT parameters affect. Full model, created by the regression and by the DACM method, was validated. It was able to predict values that were close to the actual values but not in the acceptable level. The model should be developed in order to gain more accuracy. It was noted that some factors were missing in the model and should be integrated to the model in future studies.

TIIVISTELMÄ

EMMI VÄLIMÄKI: CMT-prosessin mallinnus, simulointi ja validointi: sovellus materiaalia lisäävään valmistukseen.
Diplomityö, 63 sivua.
Helmikuu 2017
Materiaalitekniikan diplomi-insinööri tutkinto-ohjelma
Pääaine: Metallimateriaalit
Tarkastajat: Professori Eric Coatanéa and Professori Petri Vuoristo

Avainsanat: Materiaalia lisäävä valmistus, mallintaminen, DACM, CMT, suorakerrostusmenetelmät, AlSi5, 316L

Perinteinen hitsaus on herättänyt paljon kiinnostusta yhtenä materiaalia lisäävissä teknologioissa. Materiaalia lisäävien menetelmien mallintaminen ja näiden mallien kyky ennustaa lopullisen kappaleen ominaisuuksia on noussut yhdeksi tutkimuskysymykseksi. Tässä työssä hitsausteknologiana käytetään ’cold metal transfer’ menetelmää (CMT), joka nimensä mukaan on kylmempi hitsausmenetelmä verrattuna muihin valokaarihitsausmenetelmiin. CMT-prosessissa langansyötön suunta vaihtelee. Tämän seurauksena valokaari syttyy ja sammuu, jopa 50-130 Hz taajuudella. Lämmöntuonti materiaaliin vähenee merkittävästi ja lämpövaikutukset ovat pienemmät kuin muilla valokaarihitsausmenetelmillä. CMT on automaattisesti ohjautuva prosessi ja se sisältää parametreja, jotka eivät välttämättä ole niin tuttuja käyttäjälle. Yksi tämän työn tavoitteista olikin saada selkoa vähemmän tunnettuihin parametreihin. Se tehtiin yksinkertaisen regression avulla. Materiaaleina käytettiin alumiiniseosta AlSi5 ja ruostumatonta terästä AISI 316L.

Regressiomallin luomiseen apuna käytettiin Genichi Taguchin Design of Experiments-metodia. Suoritettujen testien tulokset analysoitiin varianssianalyysi (ANOVA)-menetelmällä ja näiden avulla luotiin ei-lineaarisen regression avulla kaavat kuvainnollistamaan, kuinka CMT-parametrit käyttäytyvät prosessin aikana. Regressiomallin tarkoitus oli selventää CMT-laiteen käyttäytymistä ja yksinkertaistamaan koko prosessin mallintamista.

Koko prosessin mallintaminen tehtiin dimensioanalyysikäsitemallinnus (dimensional analysis conceptual modelling, DACM) menetelmällä, joka tukee mallien rakentamista jo varhaisissa vaiheissa. Tässä työssä esitellään mallintamisen kaksi erilaista lähestymistapaa. Ensimmäinen tapa, jossa apuna käytetään teoriasta tuttuja kaavoja, ja toinen, jossa tuettua teoriaa ei tiedetä. DACM käyttää useita eri mallintamistyökaluja, kuten dimensioanalyysia ja syys-seuraussuhde teoriaa.

Malli, joka luotiin tässä työssä, ennusti lähelle mitattuja arvoja, mutta arvot eivät olleet riittävän tarkkoja. Tästä johtuen mallia tulisi vielä kehittää, jotta tarkkuus saataisiin hyväksyttävälle tasolle. Mallista löydettiin myös puutteita ja ne tulisi integroida malliin tulevaisuudessa.

PREFACE

This work was conducted at Tampere University of Technology in the department of Mechanical Engineering and Industrial Systems. I had a privileged to work with experts in their fields and in the heart of science. Hopefully this work provides a piece of knowledge in the field of science.

I would like to show gratitude for my examiners Prof. Eric Coatenéa and Prof. Petri Vuoristo for their assistance and guidance. Also a special thanks goes to Hossein Mokhtarian, who helped me with issues that I wasn't so familiar with. He gave me assistance and support when needed. I would like to thank the people in both laboratories; in Mechanical Engineering and Industrial System and in Material Science, for the help and guidance with all the equipment. I highly appreciate the selfless and kindness I received when asking for guidance.

Lastly I would like to thank my mother and father, Mirja and Matti Välimäki for unconditional love and support.

Tampere, February 22nd 2017
Emmi Välimäki

TABLE OF CONTENTS

TABLE OF FIGURES

LIST OF TABLES

NOMENCLATURE

2D	Two dimensional
3D	Three dimensional
ALC	Arc length correction
AM	Additive manufacturing
ANOVA	Analyse of variance
BC	Boost correction
BiB	Bigger is better
CMT	Cold metal transfer
CMT-ADV	Cold metal transfer- advanced
CMT-P	Cold metal transfer- pulse
CMT-PADV	Cold metal transfer- pulse advanced
CTWD	Contact-tip-work distance
DACM	Dimensional analysis conceptual model-ling
DC	Dynamic correction
DED	Direct energy deposit
DoE	Design of experiments
GMAW	Gas metal arc welding
HT	Hotstart time
MAM	Metal additive manufacturing
MIG	Metal inert gas welding
PBF	Powder bed fusion
S/L	Solid/liquid interface
S/N-RATIO	Signal to noise ratio
SDAS	Secondary dendrite arm spacing
SiB	Small is better
SLAW	Scaling law algorithm
V	Velocity
WFR	Wire feed rate

1. INTRODUCTION

As additive manufacturing is gaining more and more interest in manufacturing companies and the need for fully understanding the processes and the effect of process parameters is rising. Process parameters affects highly on the weld bead geometry, the material properties and the quality of the product. Many studies have been made on single weld bead geometry, and how the geometry effect on the mechanical properties of the material, but not on multi weld bead geometry. [1] There is a great need for knowledge of how the process parameters effect on the material quality, since many of the additive manufacture processes include several different and interacting physical phenomena, such as melting, solidification, solid state transformations, grain growth, diffusion, heat transfer, melt flow etc. [2] These phenomena effect on the materials properties, grain size, orientation and structure, porosity and mechanical properties. By optimizing process parameters the quality of the product will increase and fundamental knowledge is gained on how the process parameters effect the material properties and is there a possibility to generalize parameters for certain property.

Challenge gaining that fundamental knowledge between parameters and material properties is that it may require severe number of tests, which is not cost effective and takes lot of other resources as well. A method for early design stages is proposed in this thesis. It simplifies and visualizes the cause-effect relationships between variables. [3] It aims to find the variables that have most influence as well as the negligible ones. Method is called dimensional analysis conceptual modeling and it combines several methods, for example dimensional analysis, bond graph theory and causal rules. [4] The method requires full understanding of the process and when modeling for material perspective all the material phenomena such as solidification and growth must be acknowledged so that the model is reliable. The model will be validated with experiment and by using Taguchi's Design of Experiments. Genichi Taguchi has developed an experiment design process from design of Experiments (DoE) that tries to reduce the amount of experiments [5]. The aim is to create systems that are insensitive to factors that are hard or expensive to control. Traditional Taguchi DoE consists of three different steps; system design, parameter design and tolerance design. These steps are fundamental in order to gain the required quality. Even though Taguchi's method aims on reduce the amount of experiments needed, sometimes the complexity of the system as well as the cross effects of the parameters can increase the amount of experiments and therefore the amount of resources. With this method and the validation with DoE, we can conduct less experiments in order to gain the same or even greater knowledge of the process and the effects on the material.

The aim of this thesis is to find and understand relationships between process parameters and material properties by using the DACM and validation via Taguchi method. And, to show how these methods work and can improve design stages in a process. We studied the CMT technology and examined well-known and -used materials; stainless steel 304 and aluminum.

2. METAL ADDITIVE MANUFACTURING

American Society for Testing and materials has defined additive manufacturing as "a process of joining materials to make objects from 3D model data, usually layer upon layer, as opposed to subtractive manufacturing methodologies." [6] This manufacturing method is coming more and more commercialized although it has been around two decades. Additive manufacturing (AM) has several advantages compared to conventionally manufactured components. It decreases the product development time and cost, it is an environmentally friendly manufacturing method, reduces material usage and it highly energy efficient [7], [8]. Even though there are several advantages, it is crucial process for the produced material. Layer-by-layer building causes repeated thermal cycles that can cause differences between layers, relatively rapid solidification can result in metastable phase formation and directional cooling leads to columnar microstructure that can lead to anisotropic features. [7] Dimensional accuracy and surface quality are also drawbacks when comparing traditionally manufactured parts. [9] Usually, depending on the AM-process used, produced part needs post-processing.

2.1 Classification of MAM

Metal additive manufacturing (MAM) can be classified by the raw material; powder bed, powder feed and wire feed, or by the energy source; laser, electron beam, arc. [7] Sames et al. [10] classified AM-processes to powder bed fusion (PBF), direct energy deposition (DED), binder jetting and sheet lamination. Figure 1 is a schematic sketch of PFB process method. In the process powder is laid in a bed where the energy source melts preferred sections layer by layer forming desired shape. New powder is spread after each run. [7] According to Sames et al. [10] main challenges in PFB processes is porosity and infiltration. These effects on the chemistry of the material and there is a limited variation of alloys that can be used via this method.

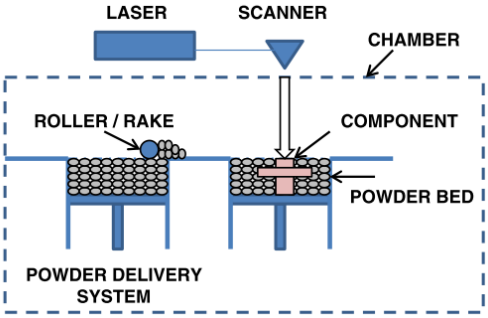

Figure 1. *Powder bed fusion process method.* [7]

DED processes differ from PFB in the way how the filler material is inserted to substrate. In PFB the material is laid on a bed, but in DED the material comes from feeder that can be integrated into the nozzle. DED processes can be referred as welding processes. In DED processes feedstock can be powder or wire. Energy sources are typically laser or electron beam, but also arc has gaining more attention. Figure 2 is presenting both powder fed and wire fed processes schematically.

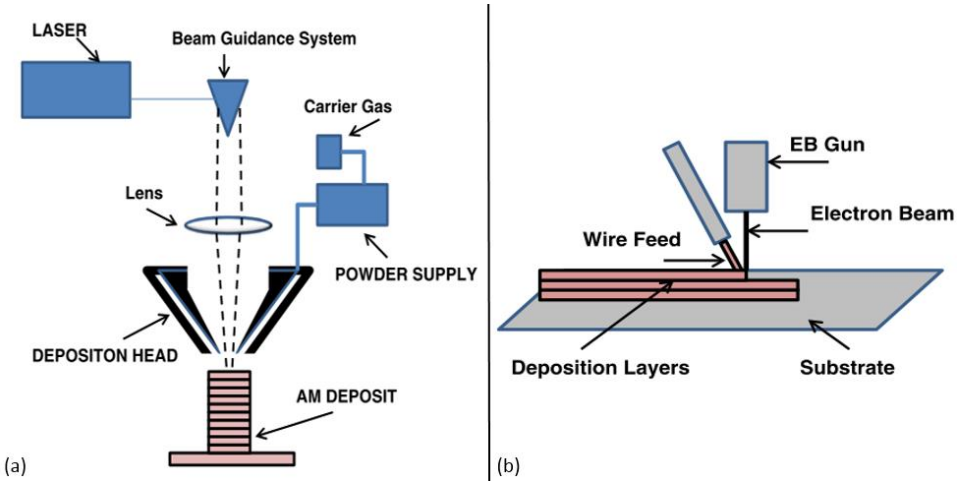

Figure 2. *Process method for powder feed (a) and wire feed (b) systems.* [7]

Binder jetting was invented by researchers at MIT. [10] In the process binder is injected on the metal powder and cured to give mechanical strength. The loose powder and the binder is disintegrated off, which gives 60% dense part. Then the part can be infiltrated or consolidated. By capillary action a second material is infiltrated to sintered parts. Consolidation is not well reported method, but according to Sames et al. [10] it can produce solid alloys.

In sheet lamination, a 3D object is sliced to 2D parts. These parts are cut from metal sheets and stacked on top of each other forming a 3D object. Layer are joined together by either adhesively of metallurgical using brazing, diffusion bonding, welding etc. [10] Its benefits are low distortion and cost, and it has relatively good surface finish. It suffers anisotropic properties, third dimensions' accuracy is hard to control, and parts joined adhesively are unreliable in shear and tensile loading conditions.

When DED-wire fed process is compared to other AM-processes, there are several differences in the designing of the product as well as in the final product. Table 1 shows the conclusion of different AM processes and their features. In powder bed fusion processes built volume and deposition rate is lower, layer thickness is smaller than in the DED processes. Built volume of powder bed manufacture process is less than 0,03 m^3, which is significantly lower when compared to the DED processes. [10] On the other hand, dimensional accuracy and surface roughness much smaller in PFB than in DED. All these features depend on the machine is used; different manufacturers have different size machines with different features. Limited possibilities to create overhangs is in DED, when

with PFB processes those are possible and one of the key advantages. With DED processes producing multi-material processes is possible, when with PFB is not. Part repairs are also possible with DED and are common, but not PFB according to Sames et al. [10].

Table 1. Comparing different features of different AM processes. [9]–[13]

		PBF		DED			Binder jetting	Sheet lamination
Process properties	Heat source	Laser	E-beam	Laser	Laser/arc	E-beam		
	Feedstock	Powder	Powder	Powder	Wire	Wire	Powder	Sheets
	Atmosphere	Inert	Vacuum	Inert	Inert	Vacuum	Open air	Open air
	Deposition rate cm^3/h	5-20	55-80	10-70;230;	700-2000; 2500	700-2000	1200-1800	
	Max. building volume m3	0,01-0,06	0,01-0,06	0,03-1,2	0,18-1,9			
	Layer thickness µm	10-100	50-200	250	1500-3000			Thickness of the sheet
	Feature size µm	75-100	100-200	360	16000			
	Dimensional accuracy mm	±0,04		±0,2	±0,2	±0,2		
	Surface roughness µm	9-10			200			
Material properties	Porosity	Low	Low	Low	Low	Low	High	Between sheets
	Cracking	Yes	Not typical	Yes	Yes	Yes	Fragile green bodies	No
	Delamination	Yes	Yes	Yes	Yes	Yes	No	Yes
	Residual stress	Yes	Low	Yes	Yes	Yes	Unknown	Unknown
Design properties	Multi-material	No	No	Possible	Possible	Possible	Infiltration	Yes
	Overhangs	Yes	Yes	Limited	Limited	Limited	Yes	Limited
	Mesh structures	Yes	Yes	No	No	No	Limited	No

There are many ways to add material on material. Every method has their advantages and disadvantages. It is important that the process is used for right application otherwise the benefits of AM are not properly exploited. For example PFB processes are excellent for geometrical complexity, customization etc. when DED processes the use might be relevant for simpler and larger geometries.

2.2 Applications for MAM

There are several industries that have been interested in additively manufactured products. Initially additive manufacturing has been an effective tool in prototyping, but it is expanding to producing end-use products. [10] Mass production of large amounts of similar parts is not suitable for additive manufacturing products yet, but technologies are advancing and process time are being reduced which will make AM more and more viable option for larger quantities. [14]

Aerospace and automotive industries have been the driving forces in MAM. These industries are making demanding parts from high-cost materials. [10] For example parts made from expensive titanium alloys. Traditionally made parts have high material waste due to the subtractive method but with MAM can be minimized. Aerospace industries have made AM brackets and landing gears. Also DED processes have been used to make turbine blade repairs and even repairing a single crystal material. Current typical applications for MAM are repairs of worn and damaged parts, prototypes during product development phases, small production of parts where other manufacturing techniques are expensive, geometrical complex parts and parts made by high cost materials. [7], [10], [14]

Another major advantage of AM is personalization. It is widely used in medical applications, dental implants, bone replacements are made for the patient to fit him or her perfectly. Also, architects, furniture, fashion and jewelry designers have taken advantage of the design freedom that some MAM techniques give.

Possibilities are expected grow when more people get involved with MAM and start to think out of the traditional way. The cost of AM-machines is not the only limitation for the process. Capability of the MAM-machines is one of them. Greater than meter-scale productions are not possible according to Sames et al. [10], even though typical welding systems are already breaking that. Also, deposition rates are slow which can be limiting feature. New processes have been taken under consideration for higher deposition rate-point-of-view and more applications and industries are getting interested. The required knowledge is not only of the process itself, but also of the microstructure and properties of the manufactured parts in order to additive manufacturing processes to evolve from prototyping to even mass manufacturing.

2.3 Cold metal transfer - CMT

Some of the AM-processes have low deposition rates and the production times can increase to even several days. Cold metal transfer, also known as CMT, was introduced by Fronius in 2004. It is a welding technic modified from gas metal arc welding (GMAW), which have given promise to the metal additive manufacturing community for higher deposition rates. [15] Many researchers have gained interest towards CMT, because conventional arc welding has an unstable arc and a lot of spattering. [16], [17] Fronius has claimed that CMT-process is the most stable weld process in the world. [18] Sequeira Almeida and Williams [15] have reported that CMT has an excellent quality on welded beads, extremely stable arc, lower heat input than the other DED-methods, and nearly spatter free process. CMT is easy to operate, handle and combine with robots [17].

2.3.1 Principle

CMT is modified from MIG-welding method. It is a “cold” process when compared to other arc welding methods. CMT can be thought as a cycle of three main phases; short-circuit phase, boost phase and burn phase. Boost and burn phase together forms the arcing phase, referring the time that the arc is on. [19] These phases are presented in Figure 3. This on/off-arcing leads to lower heat input than the traditional arc welding methods.

In typical arc welding, there are four main methods for metal transfer; globular, short-circuiting, spray and pulsed-spray, [20] but CMT has controlled dip transfer mode mechanism, where the molten droplet is dipped into the weld pool and the drawn back of the wire forces droplet to detach. The backward movement reduces significantly the spatter, since no droplets transfer from the gap between wire and base material [15]. Frequency of the backward movement can range from 50 to 130 Hz. During the droplet detachment

the process is almost current free, only heat input is taking place at the arcing period (in the Figure 3 section (3) Plasma phase) [21]. This is a great benefit compared to other methods. It lowers the heat input which leads to lower distortion and accordingly Kazanas et al. [22] could lead to even better mechanical properties.

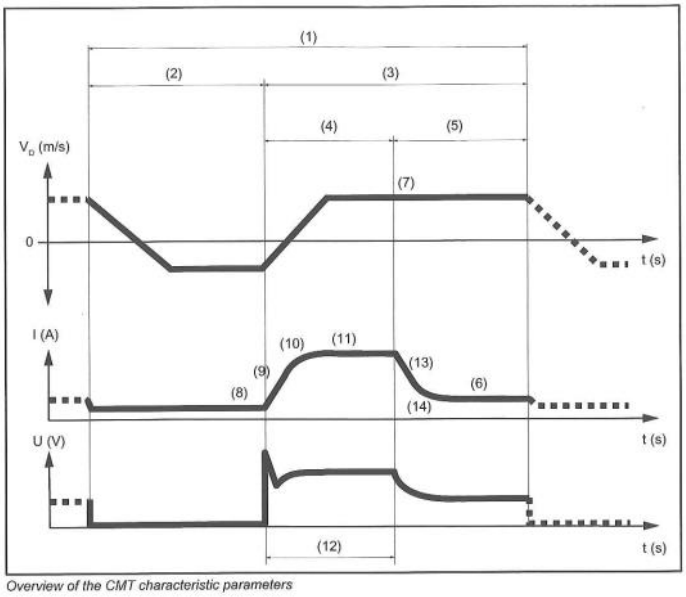

Overview of the CMT characteristic parameters

(1)	CMT cycle time	(4)	Boost phase
(2)	Short-circuit phase	(5)	Burn phase
(3)	Plasma phase		

Figure 3. CMT characteristics showing the variations of wire feed rate, current and voltage..

Figure 3 shows the characteristics shown of the traditional CMT process and Figure 4 is the basic principle of the CMT cycle shown. Mezrag et al. [19] studied the CMT cycle closely and tried to understand the effect of various parameters, such as boost current, wait current and short-circuit current, of the current waveform on the heat and metal transfer. They defined a CMT cycle by the following. When the arc is ignited, the boost phase starts, wire feed can be considered in a static position and the wire top is starting to form a liquid drop. Then starts the burn phase. Current decreases to avoid the detachment and growth of the droplet and the wire feed rate increases until it the short-circuit phase begins a.k.a. droplet touches the weld pool. The voltage of the arc is constant in the boost phase, but decreases in wait phase, since the arc length is decreased by the movement of the wire. The duration of the wait phase is determined by the time that is required the wire tip to touch the substrate material. In the short-circuit phase the voltage is near zero and the wire feed rate is backward. The backward movement forces the melted material to form a narrow bridge between the droplet and the wire and with the aid of surface tension molten droplet is detached from the wire and the arc is reignited. The duration of the short-circuit phase is dependent on the time that is required to detach the molten droplet.

After the droplet is detached the cycle starts again. One cycle happens in order of milliseconds. The reversing motion of the filler depends on the filler metal, shielding gas and diameter of the filler/electrode.

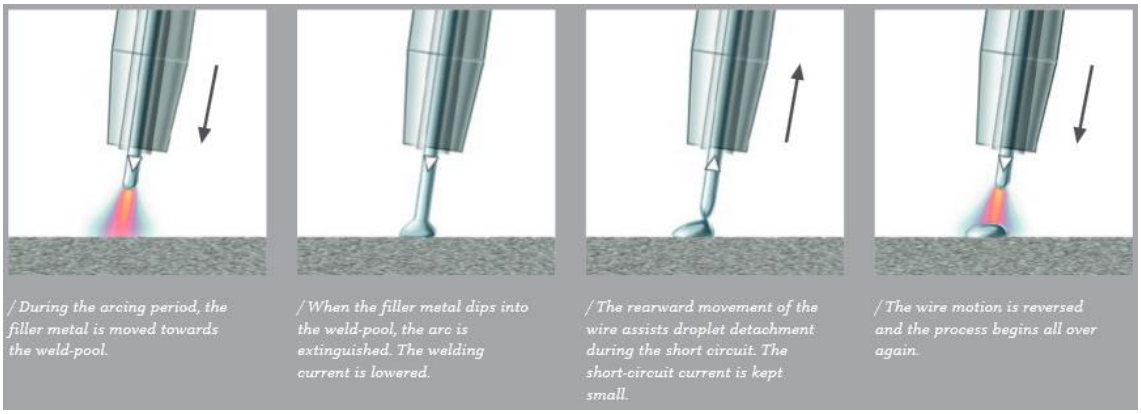

Figure 4. Cold metal transfer process. [18]

2.3.2 CMT-parameters

CMT-process can be called as a closed system. User chooses material, filler diameter, gas and the wire feed speed, Fronius's black box defines the rest. This so called black box referred as a synergic line. [23] These synergic lines have been created by Fronius via special measurement technology; oscilloscope, high-speed camera etc. for each material and diameter of the filler. Fine tuning of the synergic line can be done with parameters such as arc length correction, hot start time, dynamic correction and boost correction, these parameters varies with the filler material. Prakasham et al. [24] stated that the synergic line controls the voltage and amperage via wire feed speed linearly.

Traditionally in arc welding the length of the arc is modified by the voltage or wire feed speed but in CMT it is more complex. Arc length correction (ALC) changes the wire feed rate (WFR) in the plasma phase (in Figure 3 number (2)). Increasing ALC decreases the WFR, which have several effects. Burn phase (in Figure 3 number (5)) duration increases, which makes the short circuit phase (2) less frequent. The arc acts more like a longer arc length. Decreasing ALC has the opposite effect; increased WFR, shorter burn phase, higher short circuit frequency and it acts ore like a short arc. [25] According to Fronius's training literature long arc is beneficial when weld seam is wanted to be wide and short arc when undercut are wanted.

Other CMT-parameters are dynamic correction (DC), hot start time (HT) and boost correction (BC). The one that is possible to change depends on the filler wire, steel or aluminum. When using steel wire, dynamic correction has effect on the penetration, temperature of the weld puddle etc. It lowers the short circuit current (8), when increasing the DC value. This leads to colder weld and less penetration. Decreasing the DC increases short circuit current, which means hotter weld and possible spatter. [25] By increasing

the boost correction value, the penetration is increased, a bigger and hotter droplet is detached. Decreasing has the opposite effect. [25] Boost correction is relative when using stainless steel wires. Hotstart time affects when welding with aluminum wire. Low value of HT mean low heat input on the material at the start and by increasing the value the heat input increases as well as arc length at the start. [25]

Sequeira Almeida [26] did an extensive study on the CMT-parameters. He studied ALC and DC and their effect on the average current, voltage, wire feed rate, bead characteristics, penetration and dilution, just to name a few. Studies showed that ALC had nearly a linear relation between the current and voltage. As ALC increased, current and voltage increased. Similar effect ALC had on the power and deposition rate. Bead characteristics, such as height and width, was affect by ALC as well. For example, width increased with increasing ALC, when height was kept almost similar. His results showed that ALC is a critical parameter in controlling the deposition rate, average power and nominal arc-length. For DC, his studies showed that voltage, current, power and deposition rate decreases when DC increases. Bead characteristics were not influenced by DC. When comparing ALC to DC, extend of the effect was less in DC. The influence on arc power and deposition rate is moderate and only little effect on arc-length and bead characteristics.

Synergic line controls the CMT-process, even though the synergic line is automatically determined by the material and diameter can some fine tuning be done to the process by ALC and HT/DC/BC. Understanding those effects on produced bead is important. There has been some studies on defining those effects, [26] and in this thesis is done a simple determination for those parameters as well.

2.3.3 CMT-Methods

CMT-power source has several process possibilities. Each process has different heat inputs. According to Cong et al. [27] conventional CMT creates large amounts of pores and isn't suitable for additive manufacturing, when using aluminum wire. Fronius have improved the conventional CMT with pulse welding, advanced process and pulse advanced process.

CMT-Pulse process inputs more heat according to Fronius. [18] It has higher welding speed that conventional CMT, it's flexible and the pulses can be specified. The duration of the pulse phase as well as the pulse current affects the process and deposited material. Higher current and longer pulse means greater pulse energy, which leads to bigger pulse droplet with more energy and the pulsing frequency is lower. [25] On the other hand smaller droplet with less energy and higher frequency is created with less pulse energy, less current and shorter pulse time.

In CMT-Advanced the polarity of the process varies. It changes the cycle from positive to negative certain amount of times. With the polarity changes, thermal input is controlled

and higher deposition rate is gained. Wang et al. [28] studied the effect of the electrode positive/negative ratio on the microstructure and mechanical properties of dissimilar welded joints. They found that ratio had significant effect on the geometry sizes of the cross-section of the weld. Penetration were greatly lower when the ratio between electron positive and negative decreased and there was less base metal. Decreasing the ratio mean less heat input to the system. Willinger [25] confirms Wang's findings. The more positive cycles the higher heat input and the more negative cycles the less heat input into the system and it also increases the deposition rate. Lukkari [20] stated in his book that the differences between the polarity of the arc is duo to the fact that wire melts faster in the negative pool. This means the melted material is larger, which prevents the arcs ability to penetrate.

CMT-Advanced Pulse combines pulse cycles with CMT-ADV cycles. Pulse cycle's polarity is positive and CMT cycles is negative. CMT-Advanced gives definite precision which can be vital in additive manufacturing. Cong et al. [27] found that CMT-Advanced Pulse is the most suitable for reducing porosity in aluminum-copper alloy additive manufacturing. Advanced Pulse process is relatively new and it has not been studied widely.

These processes can be used as an additive manufacturing process. They vary in their heat inputs and for certain material other process can be more fitting than the other. These processes have not been studied effectively yet and all their benefits and drawbacks aren't known. Great knowledge is needed to clarify their prospects in additive manufacturing.

2.3.4 Safety

As in all manufacturing safety of the welder and the surrounding are very important. Arc processes are high temperature processes and there is always a fire risk. The area that is used to weld or manufacture with arc should be marked as a hot work place and the welder, who uses the process daily should have hot work permit, an occupational safety card should be as well. Arc creates radiation between short waved ultraviolet radiation approx. 100 nm to long waved infrared radiation 2000 nm. [20] These kinds of radiations can cause itch, redness and even burns to the skin. Eyes can also be damaged and welder can suffer from redness, sensitivity to light, epiphoras and pain. Eye protection is compulsory and clothes should be thick enough not to let light through. Other main issue is the welding gases. Some of the materials can create dangerous gases during welding and gas-masks should be worn. Materials that do create these kinds of gases as for example stainless steel and aluminum. Chrome and nickel from stainless steels can be irritating in high amounts as well as aluminum when welding pure aluminum or it alloys. Other important safety factors that Lukkari [20] have pointed out are the noise- and electrical safety issues, ergonomics, tidiness and order. These will help the welder to work safely and efficiently.

3. WELDING METALLURGY

As DED processes can be referred also as a welding process, metallurgy of welding can be somewhat similar as in additive manufacturing. In welding heat transfers primarily through conduction to the substrate, conduction to the substrate material and convection to the shield gas. [10] Heat flow effects the phase transformations during welding and therefore the produced materials microstructure, mechanical properties etc. Also the residual stresses and distortions are cause of heat flow.[29] The heat input of an arc process can be calculated from

$$E = \frac{U \times I}{v} \tag{1}$$

where, E is heat input, U is voltage, I is current and v is travel speed of the weld, respectably. [20] Not all the heat input go to the weld pool, some of it will transform to radiation, conduct or spatter to the environment. Some of the heat also goes to heating up the protective gas. To get the actual heat input to the weld the process efficiency must be known. Pepe et al. [30] have calculated the efficiency of the CMT processes and stated in their studies that it is approx. 85%. From this equation 1 can be formed to

$$E = \eta \frac{U \times I}{v} \tag{2}$$

where the ŋ is the efficiency of the process and the actual heat input is defined. [27]

The input heat causes material to melt. Materials that have high melting point needs more heat input and vice versa. The amount of heat input can be crucial, too high can lead to vaporization and too low to insufficient melting, both of them are cause to some defects in welding, such as porosity and areas that lack of alloying elements or decrease of the mechanical properties of the weld. [20]

3.1 Solidification

Transformations between different states of material are known as solidification and melting. [31] The mechanical properties of the weld are effected by parameters such as temperature distribution, alloying and cooling rate. The knowledge of how the mechanism of solidification and how the parameters effect is crucial for controlling the properties of the material. Solidification behavior of welds controls many things, for example grain size and shape, segregation, distribution of inclusions, porosity, hot cracks and ultimately the properties of the weld. [32] Considering the nucleation theory and solid phase growth is important to understand the development of solidification microstructure.

The differences in free energy ($G_L - G_S$) is the driving force of solidification. Melted material is cooled below its equilibrium melting temperature (T_m). [32] For liquid to solidify there is need for nucleation site, such a place can be the walls of the container or impurity particles in the liquid, this is called heterogeneous nucleation. If the liquid is undercooled more than 250 K it can nucleate spontaneously and is called homogeneous nucleation. [31] Latter demands conditions that are extremely difficult to achieve.

3.1.1 Homogeneous nucleation

When a liquid with a volume V_L with free energy G_1, as shown in Figure 5a, is put in a temperature below its melting temperature T_m, some of the atoms can cluster together and form a small solid sphere. The free energy will change to G_2.

$$G_2 = G_1 + \Delta G \tag{3}$$

where the ΔG is the change in free energy and it can be written:

$$\Delta G = -V_S \Delta G_v + A_{SL}\gamma_{SL} \tag{4}$$

V_S is volume of the solid sphere, A_{SL} is the interface between solid and liquid, and γ_{SL} is the interfacial free energy between solid and liquid phases. ΔG_v is the difference between the free energies per unit volume of solid and liquid respectively ($G_v^L - G_v^S$), as shown in Figure 6.

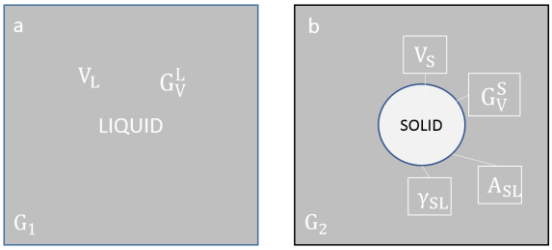

Figure 5. Homogeneous nucleation. [31] ***(modified)***

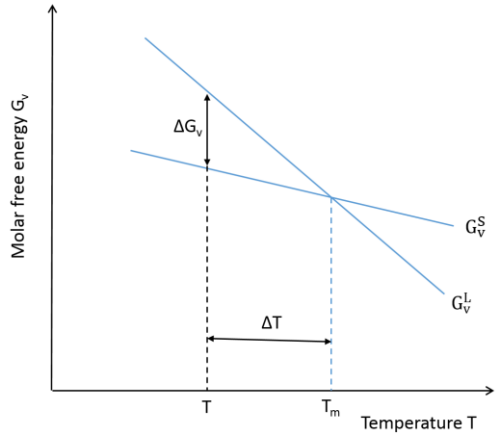

Figure 6. Difference in free energies between solid and liquid. [31] ***(modified)***

For an undercooling ΔGv can be given as

$$\Delta G_v = \frac{L_v \Delta T}{T_m} \tag{5}$$

where L_v is the latent heat of fusion per unit volume. When thinking, the solid nuclei is a sphere and give it a radius r, the equation 4 can be written as

$$\Delta G_r = -\frac{4}{3}\pi r^3 \Delta G_v + 4\pi r^2 \gamma_{SL} \tag{6}$$

This equation is schematically shown in Figure 7. From the figure, can be seen the size effect. When the nuclei are small the interfacial energy controls the solidification and the free energy would increase. These small nuclei will melt back in order to keep the free energy minimum. After a certain radius r^*, nuclei become stable and the free energy will decrease with the increase of the nuclei's radius.

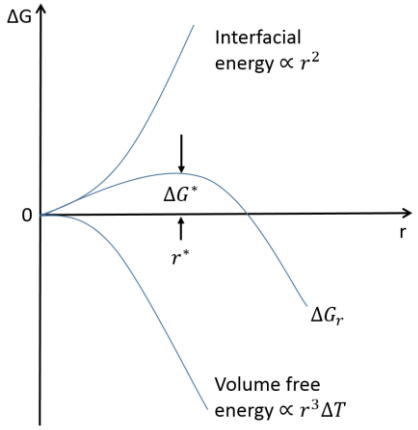

Figure 7. Homogeneous nucleation of a sphere with radius r associated with the free energy changes. [31]

There is a threshold energy ΔG^*, which requires thermal activation. When $r = r^*$ $\Delta G^* = 0$ which gives (and the substitution of ΔG_v),

$$r^* = \frac{2\gamma_{SL}}{\Delta G_v} = \left(\frac{2\gamma_{SL} T_m}{L_v}\right)\frac{1}{\Delta T} \tag{7}$$

$$\Delta G^* = \frac{16\pi\gamma_{SL}^3}{3(\Delta G_v)^2} = \left(\frac{16\pi\gamma_{SL}^3 T_m^2}{3L_v^2}\right)\frac{1}{(\Delta T)^2} \tag{8}$$

It can be seen from the equations 7 and 8 that when increasing the undercooling (ΔT) the thermodynamic barrier to homogeneous nucleation decreases (r^* and ΔG^*). When the undercooling is large enough the homogeneous nucleation can form, but there has been tests on pure liquid drops and they concluded that undercooling must be more than $0{,}2T_m$. [31] [33]

3.1.2 Heterogeneous nucleation

Nucleation is never fully random, but nuclei form in places where the effort of formation is low, such places can be mould wall or particles in a liquid etc. The Figure 8 presents the heterogeneous nucleation on a mould wall, where γ_{SM}, γ_{SL} and γ_{ML} are the interfacial tensions and θ is the wetting angle.

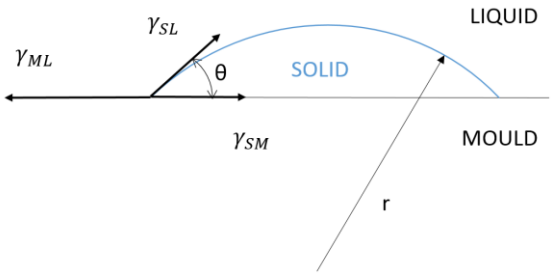

Figure 8. Heterogeneous nucleation. [31]

Heterogeneous nucleation differs from homogeneous nucleation by the factor S(θ). The factor has a numerical value ≤ 1 and it lowers the critical free energy of heterogeneous nucleation. Heterogeneous nucleation can be written,

$$\Delta G^*_{het} = \Delta G^*_{hom} S(\theta) \tag{9}$$

where

$$S(\theta) = \frac{(2 + cos\theta)(1 - cos\theta)2}{4} \tag{10}$$

Note that the factor S(θ) is only dependent on the wetting angle θ so the shape of the nuclei determines the whole factor. According to Porter et al. [31] it is called the shape factor.

3.2 Grain growth

The microstructure, as well as the grain size influence most of the mechanical properties, such as hardness, yield strength, tensile strength, fatigue strength and impact strength. They all increase with decreasing grain size. [34] To obtain the optimal grain size the grain growth plays important role. After the nucleation has taken place, the solid interface need to grow. Porter [31] pointed out that there are two different types solid/liquid (S/L) interface. First is related to metallic systems, it is atomically rough or diffuse interface and it migrate by continuous growth. Other type of interface is atomically flat of sharply defined interface, it migrates by lateral growth and it is associated with non-metal materials. S/L interfaces nature is determined by heat flow and the thermal gradients in the melt pool [32]. Usually the S/L interface is planar, but depending on the solidification

condition and the material system involved it can be also cellular or dendritic. Figure 9 shows the four basic types of S/L interface morphology.

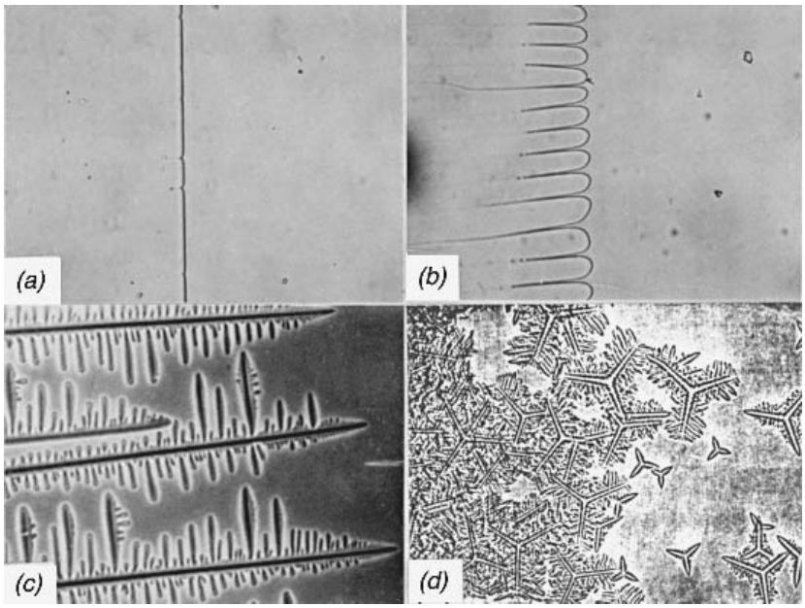

Figure 9. Solidification modes. (a) planar solidification, (b) cellular solidification, (c) columnar dendritic solidification, and (d) equiaxed dendritic solidification. [29]

The weld pool is considered moving in direction *x* with a velocity *v*. The heat extraction from the liquid to the solid causes the weld pool to experience a travelling temperature gradient *G* [35].

$$G = \frac{\partial T}{\partial x} \tag{11}$$

According to Daniels [35] the velocity of the solidification front, growth rate, is dependent on the travel velocity and the direction of growth.

$$R = v\cos\theta \tag{12}$$

Where *R* is growth rate and the *v* is the velocity of the weld pool. θ is the angle between the travel direction and the solid growth direction.

Solidification morphology is determined by the ratio between temperature gradient and growth rate, G/R. When the temperature gradient is reduced gradually below the critical value the planar interface the interface will format a cellular or dendritic structure [31]. The breakdown of a planar interface has been proposed by two different theories, constitutional supercooling and the interface stability. According to [29] interface stability considers only the thermodynamics of the problem, when the constitutional supercooling takes the interface kinetic and heat transfer under account. The composition changes in the S/L interface are the cause for constitutional supercooling.

In the Figure 10 are the effects of the ratio on solidification shown. There can be seen that with high ratios, high temperature gradient with lower growth rate, will result in planar morphology, and with low ratio it transforms to cellular or even dendritic, i.e. constitutional supercooling areas.

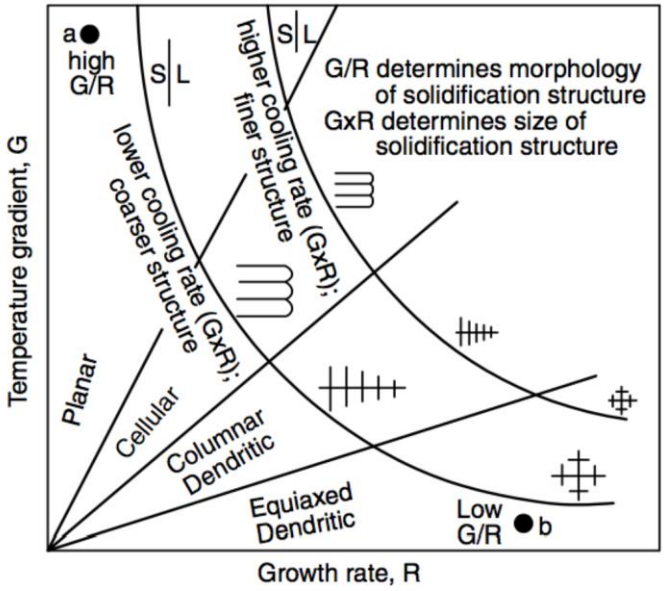

Figure 10. The effect of the ratio G/R on the solidification morphology.

From the Figure 10 can also be seen how the product of G and R, cooling rate, effects on the size of the structure. With higher rate results in finer structure and vice versa.

As can be seen the final microstructure of the primary phase is determined by the interactions of thermal gradients with the growth rate and other solidification conditions. In the final microstructure the elements such as morphology, distribution of the grains and compositional variations are influenced by the stability of the S/L interface. [32]

3.3 Effect of welding parameters

Welding speed and heat input are the most effective parameters in welding. They affect the pool shape, cooling rate and therefore the structure of the material. The grain structure is mainly cause of composition of the material, weld pool shape and the solidification parameter G/R. [36] The Figure 11 is a schematic sketch of influence of the welding speed on the pool shape. As can be seen that with low velocities the pool is more round shape and with high velocities the shape has ‘tail’. The shape is called teardrop. [29]

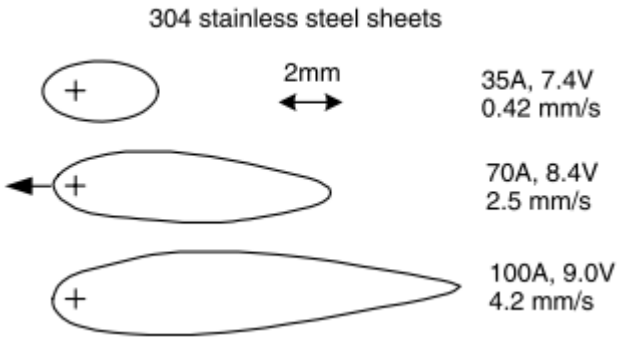

Figure 11. Effect of welding speed on pool shape in arc welding 304 stainless steel sheets.

Shape of the pool effects the grain structure. With high velocities shape is teardrop and the pool can be thought as a straight line. This will result that the columnar grains are straight as well when in low velocities shape is more round and the columnar grains will curve towards in the pool edge. This effect is illustrated in Figure 12.

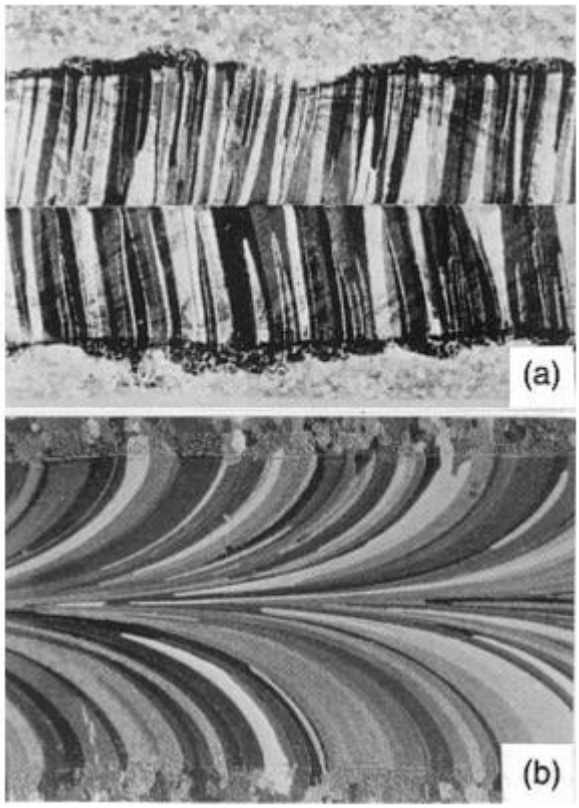

Figure 12. Illustration of the effect of welding speed on the grain structure. (a) 1000 mm/min velocity and (b) 250 mm/min velocity. [29]

The amount of heat is input per unit of length to the weld has effect on the cooling rate (R). The more heat is put in the lower cooling rate is. Cooling rate is affected by the preheat temperature as well. As has been mentioned before cooling rate has an effect on

the solidification of the material. [29] According to Rosenthal's three-dimensional equation [29] cooling rate can be expressed:

$$CR = \varepsilon = \frac{\partial T}{\partial t} = -2\pi kV\frac{(T - T_0)^2}{E} \quad (13)$$

The higher cooling rate the less time material has to solidify and finer structure is created. Structure can be either cellular or dendritic. From dendrite arms spacing, the solidification time or cooling rate can be calculated as:

$$SDAS = at_f^n = b(\varepsilon)^{-n} \quad (14)$$

where SDAS is the secondary dendrite arm spacing, t_f is the local solidification time, ε is the cooling rate, and a and b are constants. SDAS can be calculated from the microstructure of the sample by by counting the amount of dendrite arms and measuring the distance of the first and last.

4. ADDITIVE MANUFACTURING METALLURGY

During additive manufacturing material undergoes extensive thermal cycles. Each layer heats the former layer again, which can lead differences in microstructure throughout the whole part. [7] Produced metallurgy of the material is affected by the feedstock's chemistry and the thermal history. [10] Even though there are different AM processes, difference in energy source of how the filler is added, the melting metallurgical principles are the same. Solidification is responsible of phase distribution and grain morphology. Solidification kinetics are determined by the weld pool geometry which is affected by travel speed, power and size of the heat source. Thermal history, such as thermal cycling and cooling, determines phase formation, grain growth and kinetics of the precipitations. These are important to control to optimize the materials properties [37].

4.1 Microstructural evolution of AM

A typical microstructure for AM produced parts is columnar grain structures and the grains are highly oriented. The columnar grain structure is due to the heat flow in the melt pool as well as the geometry of the pool.

Sames et al. [10] stated that the microstructures vary between processes, in DED-processes the grain structure is influenced by the scan strategy and it is not always as oriented and columnar as in PBF. This difference can be related to the fact that more energy input results in a larger and deeper melt pool, which means more layers remelt and microstructure orientation and epitaxial growth is promoted. Larger pool also results in smaller thermal gradient and slower cooling [38].

Herzog et al. [39] wrote an overview article about additive manufacturing of metals. It included only the PFB processes, such as laser beam melting, electron beam melting. They stated that evolution of the microstructure is highly depended on the thermal cycle. The absorption and transformation into heat from the energy source, heats material rapidly above the melting point and then rapidly solidifies when the heat source has passed on. Movement of the energy source creates several re-heating and -cooling processes. This will lead to metastable microstructure and non-equilibrium compositions of the resulting phases. These features can vary upon layers, since there is different number of recycles.

When comparing AM produced parts to casted parts, it can be said that the microstructure is more fine grained, due to the rapid solidification. Thermal gradient is one of the key factors in microstructure evolution. [39] In AM thermal gradient is affected by many factors, e.g. process parameters, such as energy density, and thickness of the layer. The ambient material has an effect on the gradient, especially in powder bed processes, when the

conduction to the powder is relevant. Also, the geometry of the part influences the microstructure. Raghavan et al. [40] tried to understand the transient phenomena of repeated melting and solidification during EBM process in their studies. They created a numerical model to find the influences of the input parameters to volume fraction of equiaxed grains. Conclusion was that the diameter of the beam had an insignificant effect when the preheating had the most significant influence. They also stated that the grain morphology depends on local solidification conditions, such as thermal gradient and growth rate of the liquid-solid interface.

4.1.1 Defects

Sames et al. [10] have listed typical defects for DED-wire fed-processes. According to them processes have low porosity and poor but smooth surface finish. On the other hand, residual stress, cracking and delamination are defects that are major concern. Typically, porosity is one of the crucial defects in additively manufactured components. It effects the mechanical properties and the durability of the material. In powder bed and feed processes porosity is more common than in wire fed but according to Zhan et al. [16] pores has been detected also in CMT as well. Figure 13 shows the pores in additively manufactured aluminum wall produced by CMT.

Figure 13. Porosity of ER2319 aluminum alloy wire produced by CMT. [41]

The mechanism for pore formation in CMT, as in welding, is gas entrapping. This means that the pores/gas cannot escape the weld fast enough before solidification is completed, so they are entrapped. Due to the high velocity of the weld this is more common, but with

lower welding velocity gas bubbles have more time to escape and less pores are entrapped.

There can also be process-induced porosity, which is cause of an insufficient energy input. [10] It causes incomplete melting or spatters. The pores formed this way are not spherical and can have variety of sizes. When the energy input is too low it causes so called lack of fusion, which means the filler material is not fully melted. This is more typical for powder process systems. When the energy input is too high it is called keyhole formation. Keyhole formation causes spatter and can produce a trail of voids. Porosity can be reduced by optimizing the process parameters, especially energy input related parameters, such as travel speed, power etc.

The other major defects are residual stresses; they can be formed by mechanically or thermally. In additive manufacturing, due to the extensive thermal cycles different cooling times causes residual stresses in the material. They are formed due to both plastic transformations and the volume changes which are related to the phase changes. [33] Residual stresses can be unwanted but they also can be useful. For example, compressions stress can increase the fatigue durability, when tensile stress increases the risk for brittle fracture, and is the cause of cracking in most cases. Measuring residual stresses can be difficult and expensive. There are two main methods to measure, destructive and non-destructive. Destructive is an expensive method and the product is destroyed in the process. non-destructive methods are based on X-ray diffraction, ultrasound or magnetic method. [33] Residual stresses can be released by force or by heating. Stress relief annealing is based on the dependence of the yield strength on temperature.

In additive manufacturing anisotropy is a major concern. Unidirectional heat flow into building plate forms textured grains and anisotropic properties. [42] Texture in material science means that polycrystalline material grains have preferential crystallographic orientation. [43] When the grains have crystallographic oriented in the same direction part will have directional properties, which is called anisotropy. Even tough single grain might be anisotropic, but when there are several randomly oriented grains degree of anisotropy decreases.

4.1.2 Mechanical properties

Mechanical properties are influenced by the microstructure of the material, as well as the defects that have been created during processing. The performance of the material is dependent on the mechanical properties and therefore important to measure and understand. Typically, AM produced part has an oriented grain structure, which can mean that the mechanical properties differ in direction. For this reason, when test results are presented it is important to present the orientation of the build as well, since it is relative to the test direction.

Defects such as porosity has great effect on the tensile properties. For example, Wang et al. [44] found that entrapped pores effected the fatigue properties leading to early failures. Pores effect on the elongation of the material due to the fact that the pores reduce the affecting surface area. Ding et al. [13] stated that the hardness profiles of laser AM produced walls were slightly different depending on the travel speed. Higher speed resulted slightly higher hardness. Although their studies also showed that the post-treatment were more effecting on the hardness than the process parameters itself. Tensile properties were better in the direction of the build than across the direction of the built. This is due to the anisotropic features of the build. Mechanical properties of AM produced parts can be said to be similar as parts that are casted or wrought. Post heat treatments effect greatly on the hardness and tensile strength is highly affected by the direction of the built.

4.2 Effect of process parameters

To produce good quality products, the knowledge of parameters effects is essential. Hassenberg [21] studied parameters effect on single welded bead. According to him the most influential parameters on overall quality are welding current, polarity, arc voltage, travel speed, wire extension, torch angle and wire diameter. Amine et al. [45] investigated effect of process parameters on multilayer builds by direct metal deposition. They found that most effective parameters on microstructure and hardness was travel speed and laser power. Energy input, wire feed rate, travel speed, deposition pattern and deposition sequences are also said to have great influence on the material and relations should be fully understood. [13]

4.2.1 Wire feed rate

The wire feed rate and current must be in balance with the voltage in order to keep the arc stable. In CMT this is controlled via the synergic lines, which are also dependent on the thermal and electrical resistivity of the filler wire. [21] Typically the wire feed rate is limited by the energy of the heat source. When there is high wire feed rate, the energy used has to be high as well in order to fully melt the particle. In traditional arc welding as well as in CMT the bead geometry is highly affected by wire feed rate and the ratio between WFR and travel speed. [46] The increase of wire feed rate results more material input to the system and depending on the travel speed it determines how much material is input per unit of length.

4.2.2 Arc length

There are three main parameters when considering the concept of arc length; arc length, contact-tip-work distance (CTWD), stick-out of the wire. Arc length is the distance from the melting electrode tip and the base metal, contact-tip-work distance is the distance of the nozzle from the base metal, and last is arc length variable is the stick-out of the wire,

which is the length of how much wire is sticking out from the nozzle. [21] If the voltage is increased it will create longer arc. Porosity, spatter and undercuts are result from immoderate high voltage. According to Lukkari [20] increase of the CTWD decreases the current and also the penetration of the arc. Reason for this is that the longer stick out is the bigger resistance the wire has. As the CTWD increases the arc voltage and the length should increase in conventional arc welding [21], in CMT is more complex system. Arc length is tried to keep constant by the movement the wire and wire feed rate. The welding current and voltage are adjusted by the changes. If the distance becomes shorter, the voltage decreases and current increases. Sequeira Almeida [26] studied also the effect of contact-tip-work distance (CTWD) in CMT-process. He stated that CTWD had an important effect on the power, it increases with the CTWD.

4.2.3 Travel speed

Travel speed is the velocity of the nozzle. It has significant effect on thermal characteristics of the welding process. Cong et al. [47] studied the effect of the electron beam speed on the microstructure of a Ti-6Al-4V. They found that the velocity has a significant effect on the peak temperature and the temperature averages. The slower the velocity was the higher the peak temperature and higher average temperature. The increase of the velocity decreased the width of the bead as well as the microstructural features such as the width of columnar structures. The greater velocity the more the material tended to form columnar grain structures. More nuclei's can generate because the cooling rate increases which means a greater undercooling has taken place. During solidification the increased cooling rate could result in material with finer grains [45].

Travel speed has other main effects on the bead quality as well as microstructure. It effects also on the microhardness and wear resistance. According to Mahamood et al. [48] by increasing the velocity the microhardness also increased as well as the wear resistance of the samples in laser-powder processes. Zhang et al. [16] studied the effect of welding speed on microstructure of CMT deposited magnesium alloy clad. They stated that low velocity gives more time for the weld to solidify, which means the pores have more time to escape from the weld. Also, they stated the increase of welding velocity means less heat input into the material. That means smaller grain size due to the lower maximum temperature and the higher cooling rate. Travel speed also has a major effect on the wall quality. Kazanas et al. [22] studied the CMT and its parameters and found that increasing the nozzle velocity decreases the wall waviness up to a certain point. The deterioration of the wall quality increases after certain increase in travel speed. This was also found by Mahamood et al. [48] in their studies.

4.2.4 Other parameters

One of the parameters that highly affect the produced bead shape and penetration is the orientation of the welding nozzle. Nozzle can be set either drag, push or vertically. With drag method the penetration increases and the bead is more convex and narrower. [21] In push method penetration decreases and the bead is wider and flatter in the push method. Table 2 presents the several parameters and their effect on penetration, deposition rate and bead characteristics shown. Bead characteristics are influenced mainly by the power, wire feed rate and travel speed according to Ding et al. [13].

Table 2. Effect of process parameters on features. [21]

	Desired Changes							
Welding variables to change	Penetration		Deposition rate		Bead size		Bead width	
	Increase	Decrease	Increase	Decrease	Increase	Decrease	Increase	Decrease
Current and WFR	Increase	Decrease	Increase	Decrease	Increase	Decrease	Little effect	Little effect
Voltage	No effect	No effect	Little effect	Little effect	Little effect	Little effect	Increase	Decrease
Travel speed	No effect	Noeffect	Little effect	Little effect	Decrease	Increase	Decrease	Increase
Electrode extension	Decrease	Increase	Increase	Decrease	Increase	Decrease	Decrease	Increase
Electrode diameter	Decrease	Increase	Decrease	Increase	Little effect	Little effect	Little effect	Little effect
Shield gas %	Increase	Decrease	Little effect	Little effect	Little effect	Little effect	Increase	Decrease
Torch angle	Drag	Push	Little effect	Little effect	Little effect	Little effect	Push	Drag

Ding et al. [13] stated that the width is mainly influenced by the power and the height varies with the travel speed. Increasing the power would result wider but lower beam and increasing the travel speed result in higher but narrower bead. There are several parameters the should be taken under consideration. Also, the cross effects of those parameters should be determined. Especially in CMT parameters effect on each other and the real effect is different to determine. When changing the WFR, the arc length, voltage and current is changed via synergic lines. These have several effects on the final quality of the produced part, in microstructure point of view as well as in macrostructural level.

4.3 Materials in AM

Materials that have been studied in wire based AM-processes are mainly Fe-, Ti- and Al-based materials. [13] Aerospace industries have pushed especially Ti-6Al-4V for more research, but other materials are getting more and more attention. In this thesis, the focus is on stainless steel 316L and aluminum alloy AlSi5. Those materials have been studied but not excessively in CMT.

4.3.1 Austenitic stainless steels 316L in AM

According to Herzog et al. [39] the microstructure of AM produced parts depends not only on the process parameters but also the process itself. Typically, austenitic steels, like 316L have fully austenitic structure. This was gained in PFB process, when in DED-process structure had ~10,9 % retained δ-ferrite. Majumdar et al. [49] studied 316L microstructure in laser AM-process. They found that the microstructure was equiaxed near

the surface, between layers it was columnar and near the substrate it was fine columnar structure. Herzog explains this effect by heat conduction. [39] Lower heat conduction is experienced in the build structure than close to the substrate.

Amine et al. [45] studied process parameters effect on multilayer builds. Process was DED with powder. They resulted in large, elongated grains, that grew epitaxially. They also examined secondary dendrite arm spacing (SDAS) and how it is influenced by process parameters. They found that an increase in travel speed decreased SDAS. Increase of SDAS was reported when the heat input was increased. As the SDAS decreased the cooling rate increased. By the decrease of the cooling rate the small dendrite arms had time to solvent and SDAS increased. Typically, as SDAS decreases the hardness increases due to the increase of cooling rate, but Amine et al. [45] didn't observed anything related.

4.3.2 Aluminum alloy AlSi5 in AM

Herzog et al. [39] reported of aluminum and its alloys and their microstructures. AlSi12 had an extremely fine microstructure, and the silicon along the cellular boundaries. The layers consisted two different areas; coarse dendritic areas and fine cellular structures. These areas alternate with each other, but they disappeared on the higher layers, according to the study this was cause of the slower cooling rates and the fine cellular area had time to grow. Same effect as in steels.

Gu et al. [41] studied different CMT methods for ER2319 aluminum. They stated that one of the main challenges with aluminum is porosity and solidification cracks, CMT technologies could make using aluminum more sensible. Results indicated when comparing CMT-P and CMT-PADV, the latter is more suitable. CMT-P had many small pores due to the narrow finger shaped molten pool which prevents, according to Gu et al. the escape of gas pores. CMT-PADV had little or none pores in the built wall. Grain size is also affected by the method, it can be seen in the Figure 14. With CMT-P the grains have more columnar structure and it is aligned to the heat flow direction. CMT-PADV has lower heat input and the grains fine and equiaxed and no dilution. Also, the polarity changes affect the deposits quality. It cleans the end of the wire and reduces the hydrogen content in the weld pool.

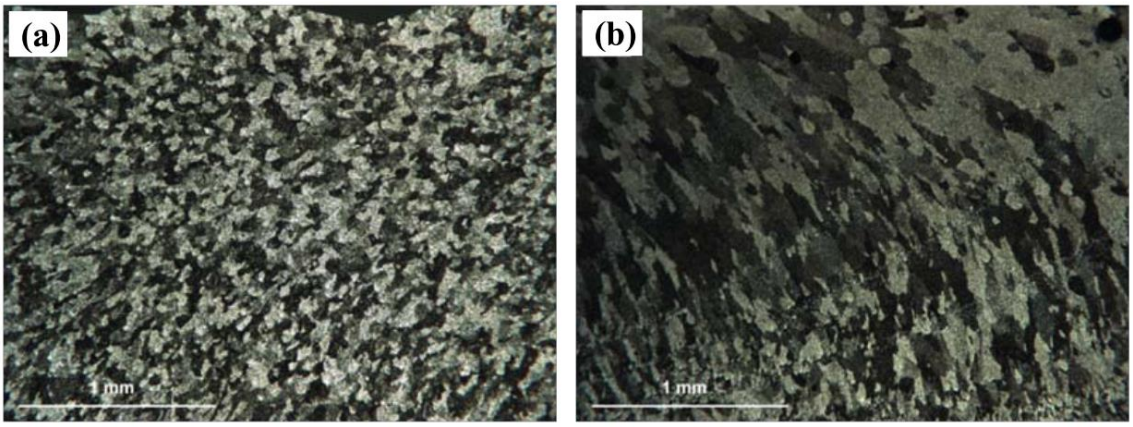

Figure 14. Microstructures of 2319 aluminum deposited by (a) CMT-PADV and (b) CMT-P processes. [41]

In Cong's et al [27] studies they manufactured thin walls from AL-6,5%Cu-alloy and found the same results as Gu et al. CMT-PADV is most suitable process for aluminum when comparing all the CMT-methods and other arc processing methods. With great control of the heat input walls with no pores can be manufactured.

5. DIMENSIONAL ANALYSIS CONCEPTUAL MODELING

DACM is a method formed from traditional modeling method such as dimensional analysis, bond graphs and causal rules. The aim of the DACM and its framework steps is to plan and optimize the experimental process so that less experiments are required to generate the model. It visualizes and simplifies the process and already from those steps can some conclusions be made. It tries to find the most influential parameters for the system and also the negligible ones, so the when conducting the validation by DoE can already some of the parameters be dismissed.

5.1 Framework steps

There are nine framework steps that the DACM process can be summarized. Figure 15 shows all the steps for the DACM process. [3] Firstly, objectives of the model need to be defined and clarified and the borders of it as well. Then functional structure of the system is created by function modelling. It tries to show the architecture of the system from the functionality perspective. Functions are presented in a box with a verb of action. This step can be crucial in DACM since the reliability is highly depended on the functional model. Variables that are effecting in the system are imported to the functional model. These variables are presented with different colours. Every colour has a meaning; black is for variables that cannot be changed unless changing the borders of the system, also known as exogenous variables. Green colour is for independent variables. They are not influenced by any other variable in the system. Variables that are difficult to control or are affected by other variables in the system are coloured in blue, dependent variables. Red are the target variables, the ones are used to evaluate the system, also known as performance variables. [4] These variables are being tried to either minimize, maximize or set target value.

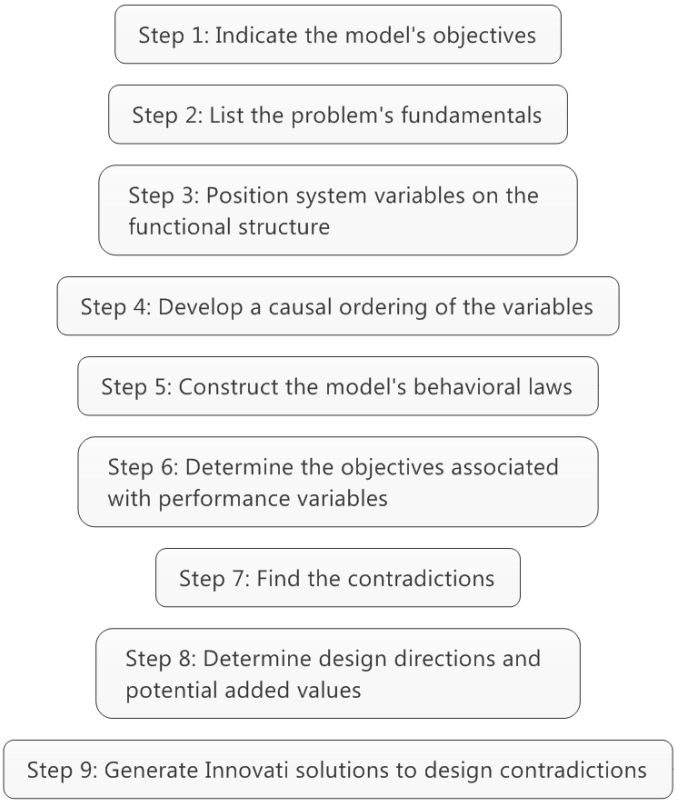

Figure 15. DACM-model's framework steps.

Next step, step 4, can be a crucial part of the modeling since it requires great knowledge of the functions taking place in the system. [3] The creation of bond graph requires the use of causal rules. Bond graph is a graphical representation of the system. It is composed from limited amount of elements, source of flow, source of effort, transformer, gyrator, flow junction, effort junction, inertia, capacitor and resistor, which are linked together by bonds. These bonds represents power that contains flow and effort. Main idea is to benefit from the representation of bond graph from existing causality rules. When this transformation from functional presentation to bond graph has been made causal roles between variables can be applied. Causal rules enable to extract the causal relation between the system variables. These causal relations between the variables and their units enables the construction of the model's behavioral laws. These laws are developed using dimensional analysis approach. Dimensional analysis is an approach where the complexity of modelling problems is reduced. It uses the dimensions of the variables and tries to conclude some relationships among the variables by creating dimensionless products π_k, that takes a form of

$$\pi_k = y_i \times x_j^{\alpha_{ij}} \times x_l^{\alpha_{il}} \times x_m^{\alpha_{ml}}, \tag{15}$$

where x_i is repeating variables, y_i is a performance variables and α_{ij} are exponents.

To create these dimensionless products Bhaskar and Nigam [50] have developed mathematical machinery to reason about a system using the type of relationship derived from equation 15. These dimensionless groups can be expressed

$$y_i = \pi_k \times x_j^{-\alpha_{ij}} \times x_l^{-\alpha_{il}} \times x_m^{-\alpha_{ml}} \tag{16}$$

and when divided by x_j the equation 16 takes a form

$$\frac{y_i}{x_j} = \pi_k \times \frac{x_j^{-\alpha_{ij}}}{x_j} \times \frac{x_l^{-\alpha_{il}}}{x_j} \times \frac{x_m^{-\alpha_{ml}}}{x_j} \tag{17}$$

From the equation 16, can be written a partial derivative including variables y_i and x_i taking the form

$$\frac{\partial y_i}{\partial x_j} = -\pi_k \times \alpha_{ij} \frac{x_j^{-\alpha_{ij}}}{x_j} \times \frac{x_l^{-\alpha_{il}}}{x_j} \times \frac{x_m^{-\alpha_{ml}}}{x_j} \tag{18}$$

Then the partial derivative can be simplified by adding equation 17 into 18 resulting in

$$\frac{\partial y_i}{\partial x_j} = -\alpha_{ij} \frac{y_i}{x_j} \tag{19}$$

From this, by verifying the sign of $-\alpha_{ij} \frac{y_i}{x_j}$, qualitative objectives can be propagated into a graph. Those objectives can be minimized, maximized or deviation from a target value can be analyzed [3].

In the second type of simulation experimental studies are supported by an algorithm called SLAW. It is based on the scaling laws and it has two main abilities. [51] First is to rank the importance of the system variables and second is to find the simple scaling law that rules the engineering problem. According to Mendez and Ordoñez SLAW algorithm is far more useful than dimensional analysis and linear regression, even though the SLAW is based on these two methods. That is based on the fact that SLAW is able to detect significant parameters that in usual situations complex problem is explained by.

Those frameworks can be used at early stages when little information is available. This is an efficient approach to start analyzing problems and understanding complex phenomena.

5.2 Validation by Taguchi method

Design of Experiment (DoE) was introduced in the early 1920's by Sir R.A. Fisher in England. He wanted to find the perfect combination of water, rain, soil, sunshine and fertilizer to produce the best corp. [52] He was able to study the effect of multiple factors

simultaneously. Since that time there has been a lot of developments in the academic world and one of the developers, Genichi Taguchi had the most significant effect on DoE.

Genichi Taguchi was a Japanese engineer that effected significantly the quality control and experimental design in the 80's and 90's. [53] He defined quality as the variation from the target value and developed a statistical method to improve the quality of products or processes, The Taguchi method. [54] It is a modified and standardized form of DoE with special application principles. [52] Taguchi wanted to create DoE that is easier, friendlier and more useful. He did that by defining quality in general terms and by standardizing the application method. Method aims to design robust systems, which are insensitive to factors that are hard or impossible to control, also known as noise factors. It is a powerful, systematic and efficient tool to optimize designs for performance, cost and quality according to Tarng and Yang [5]. Taguchi method reduces the amount of experiments, which leads to reduced time and cost, by special design of orthogonal arrays. It has three phases: system design, parameter design and tolerance design. Each phase is important to achieve the target value and the experiments should be properly planned, executed and analyzed [55].

5.2.1 Phases

System design is the first phase of the process. It involves creativity and innovations combined with great knowledge of the process and the aim is to produce a basic functional prototype design. [5], [54] It includes product design stage; material selection, components, tentative product parameter values, and the process design stage; selection of production equipment, tentative process parameter values and the analysis of processing sequences. Achieving high quality without increasing cost the parameters design phase is the key. It is a phase, where the parameter settings are determined for producing the best levels of quality with limited variation. [54] It reduces the sensitivity to the variation of environmental condition and other noise factors. [5], [53] The final phase of Taguchi method is the tolerance design. Tolerances are given to the optimal setting that have gained from the parameter design phase. Narrow tolerances commonly increases the manufacturing costs and on the other hand wide increases performance variation. [56]

5.2.2 Experiments

The impact of factors to the objective is each different. Taguchi method is a simple and systematic method to show the impact of inputs to the outputs. In this thesis, a three-level Taguchi orthogonal array table was used, but in the Figure 16 is the typical orthogonal array presented. Each row presents the number of the experiment. [56] Columns are the factors chosen in the DoE. Inside the array are levels for each factor presented. Levels of each factors can be determined. It requires deep understanding of the process. Maximum,

minimum and current values of the parameters should be known. If the values have large range more levels can be chosen and if it is small fewer levels is needed. [54]

Experiment nro.	Factors				
	A	A	A	A	…
	A	B	B	B	…
	A	C	C	C	…
	B	A	B	C	…
	B	B	C	B	…
	B	C	A	A	…
	C	A	C	B	…
	…	…	…	…	

Figure 16. Example of orthogonal array.

Selecting the Taguchi orthogonal array can be determined by the degree of freedom (DOF). DOF is calculated for each factor's levels and their sum is the total DOF. In this case each four factors have three levels, which means each factor has a DOF of 2. In total DOF is eight. This means the number of experiment runs has to be over eight. [55] Analyzing data can be done by the statistical analysis of variance (ANOVA). [5] ANOVA's initial purpose is to by measured sum of the square deviations from the mean value to separate the total variability of the data. [56] With this method can be seen which of the process parameters are the most significant statistically and the prediction of the optimal combination of the process parameters can be done. [57]

6. EXPERIMENTAL

In this thesis, the experimental part can be divided into three sections; experiments of the CMT parameters, DACM of CMT and material evaluation. First is the clarifying experiments of the CMT machinery, then is the modelling section where is used the DACM and the DoE for the optimal parameters selection and the validation of the model. After is the microstructure and mechanical performance evaluation of the produced materials. Materials used were austenitic stainless steel 316L and aluminum alloy AlSi5.

6.1 Equipment

Basic equipment of a CMT with a robotic arm is presented in the Figure 17. Unique feature in CMT compared to conventional GMAW is that it has two separate wire-controls, front (in the Figure 17 number 6) and rear (number 5). Wire feeder feeds the wire continuously and the front-wire-control, that is located in the torch, moves the wire back and forth. These units are separated with wire buffer. Its purpose is to ensure the wire feed is uninterrupted.

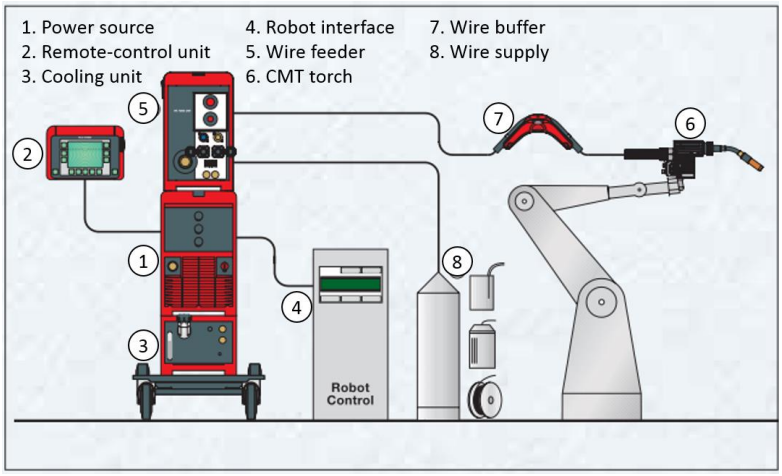

Figure 17. CMT process equipment. [58] ***(Modified)***

Remote-control unit is Fronius's own RCU 5000i, where the power source can be selected as well as for the determination of the pre-settings. TUT's power source is TransPuls Synergic 5000 CMT, where are several processes in addition to the CMT processes, for example MIG brazing, MIG/MAG standard welding, MIG/MAG pulse welding and TIG DC-welding. In the Table 3 is presented the technical data of a typical TransPuls Synergic 5000 CMT apparatus.

Table 3. Technical data of a TransPuls Synergic 5000 CMT. [59]

Technical Data			
Mains voltage	3 x 400 V	Open-circuit voltage	70 V
Mains voltage tolerance	+ 15 % / - 15 %	Working voltage MIG/MAG	14,2 - 39,0 V
Mains frequency	50 / 60 Hz	Working voltage TIG	10,1 - 30,0 V
Mains fuse protection	35 A	Working voltage Electrode	20,4 - 40,0 V
Primary continuous current (100 %)	18 - 29,5 A	Protection	IP 23
Primary continuous power	13,1 kVA	Type of cooling	AF
Cos phi (Power factor)	0,99	Insulation class	F
Degree of efficiency	90 %	Dimensions l/w/h	625/290/475 mm
Welding current range MIG/MAG	3 - 500 A	Weight	35,6 kg
Welding current range TIG	3 - 500 A	Marks of conformity	CE
Welding current range, electrode	10 - 500 A	Marks of conformity	CSA
Duty cycle at 10 min/40° C	40 % d.c. at 500 A	Safety	S
Duty cycle at 10 min/40° C	100 % d.c. at 360 A		

In the TUT facility the CMT power source is connected to ABB's IRB 4600 robot hand and to a IRBP/D2009 robotic table. Robots are presented in the Figure 18.

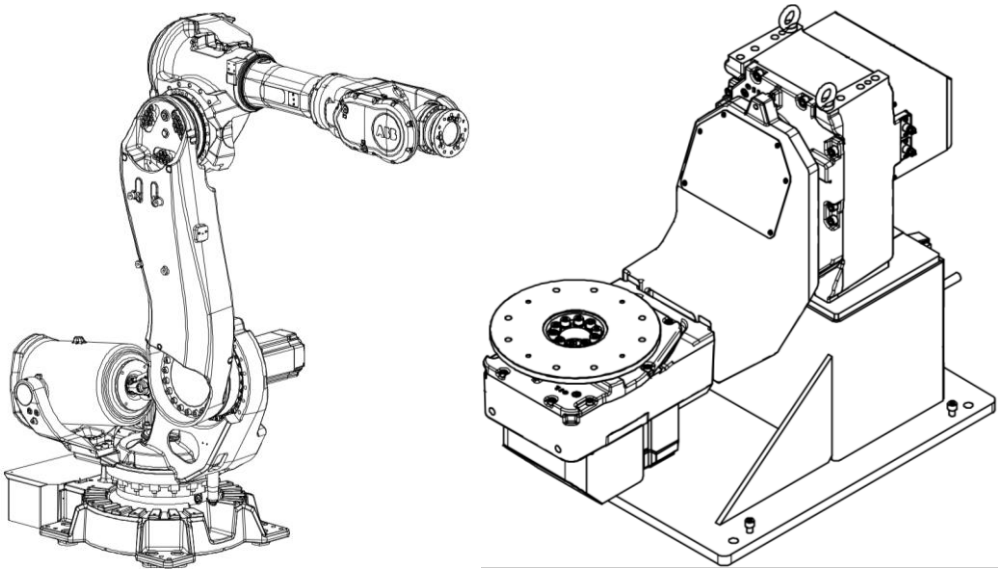

Figure 18. IRB 4600 and IRBP/D2009. [60], [61]

6.2 Material evaluation

Material composition and properties for both metals are presented in Table 4 and Table 5.

Table 4. Standard composition of AISI 316L-steel. [62]

wt-%	C	Cr	Mn	Ni	P	S	Si	Mo	N	Fe
316L	0,03	16,00-18,00	2,00	10,00-14,00	0,045	0,030	0,75	2,00-3,00	0,10	Balance

Table 5. Mechanical and thermal properties of 316L steel and AlSi5. [62] [63]

Mechanical properties	**316L**	**AlSi 5 ø1,2**
Hardness Vickers HV	155	87
Ultimate tensile strength MPa	558	110
Yield tensile strength MPa	290	55
Elongation at break %	50	29
Modulus of Elasticity GPa	193	-
Charpy Impact J	103	-
Density g/cm3	7,99	2,68
Thermal properties		
Specific heat capacity J/gK	500	-
Thermal conductivity W/mK	16,2	-
Melting point °C	1371-1399	575-630
Solidus °C	1375	575
Liquidus °C	1400	630

6.2.1 Sample preparation

Each bead had microscope and hardness test evaluations. For those examinations samples were prepared in the Laboratory of Material Science. A cross section of the beam was cut and placed in a PolyFast powder. Then it was compressed into the shape of disk in order to make the sample easier to handle for further examinations. Each sample was then grinded and polished to get unwanted scratches and stains out of the structure. After reaching good quality for the surface samples were cleaned with ultrasound for 3 minutes. In the tables below are seen the grinding and polishing parameters for aluminum and steel.

Table 6. Grinding and polishing parameters for steels.

Surface	Diamond etc.	Lubricant	Weight (N)	Time (min)
500	-	water	20	x*1
1200	-	water	20	1
2000	-	water	20	1
4000	-	water	20	1
MD-Nap	Nap B	-	20	4
MD-Chem	OP-U	-/water	20	1+1

Table 7. Grinding and polishing parameters for aluminums.

Surface	Diamond etc.	Lubricant	Weight (N)	Time (min)
500	-	water	15	x*1
1200	-	water	15	1
2000	-	water	15	1
MD-Mol	Mol R 3µm	-	15	3
MD-Chem	OP-U	-/water	15	(1*1)*2

Each sample went through microscope evaluation as well as Vickers hardness measurements.

6.2.2 Hardness test

For every bead a hardness test was carried through with Laboratory of Material Science's microhardness measurement device Matsuzawa MMT-X7. Hardness was measured from the bead in three different position. On top of the bead, from the root and in the base material, shown in Figure 19. The load for each measurement was 2942mN and it was held there for 10 second. With the device, the Vickers hardness was calculated. Each material had in total 27 measurements.

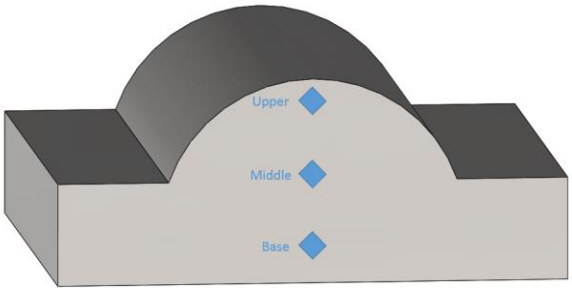

Figure 19. Positions of hardness tests.

6.2.3 Microscopy

Each sample was examined in a microscope.

Table 8 shows the plan of imaging. Depending on the amount of penetration each sample had the more images was needed.

Table 8. Samples imaging plan.

Image	Magnification	Function
1	5x	Overview
2	5x	Overview
3+n	5x	Overview
4	10x	Porosity
5	50X	Microstructure
6	100x	Microstructure

Images for porosity and microstructure were taken in the middle of the bead sample, in order to limit the possible edge defects.

6.3 DACM for single bead

In this thesis two modeling paths using DACM can be used. One from already know theories and their equations and the other were no equations can be found beforehand. Both paths are presented in the Figure 20. Modelling path 1 in the figure is presenting the modeling process where already known equations are used to generate the causal graph. This means that the modeling process starts first from equations. Then a functional model is created. The variables of the equations are allocated to the different functions. A causal graph is finally produced by taking into account both the equations and the allocation of the variables in the functional model.

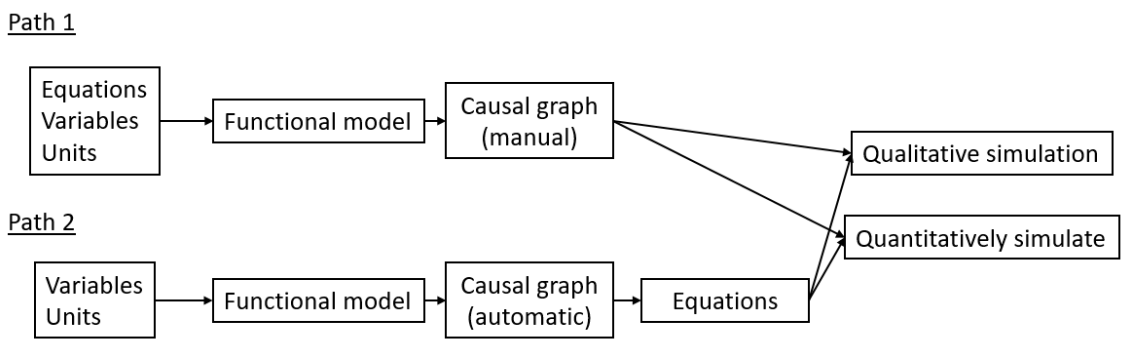

Figure 20. Modelling paths.

For example, a very well-known equation for arc welding is Equation 2. From this equation, a functional graph, can be created. Since power of an electrical system can be calculated by P=I×U the heat input can be expressed in E = (ŋ×I×U)/V. The variables are first added to the functional model presenting the process of heat creation. A causal graph is derived from the combined causal information provided by the equations and by the location of the variables on the functional model. The result is a causal graph presented in Figure 21. Power is affected by the current, voltage and efficiency of the machine, when heat input is affected by the power and the welding speed. Also, the solidification section of the model was modelled using equation 13 and this modeling path is also exemplifying the modeling path 1.

Equations 2 and for power:

$$E = \eta \frac{U \times I}{v} \qquad P = IU$$

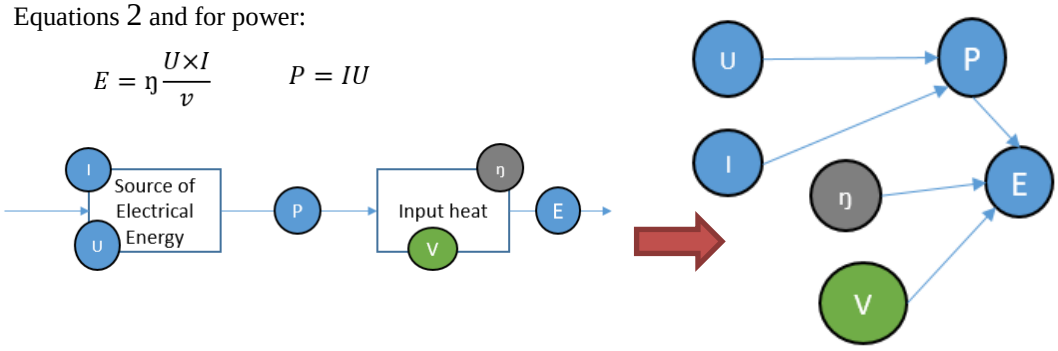

Figure 21. Presentation of functional model and causal graph for equation 2.

Equation 13:

$$CR = \varepsilon = \frac{\partial T}{\partial t} = -2\pi k V \frac{(T - T_0)^2}{E}$$

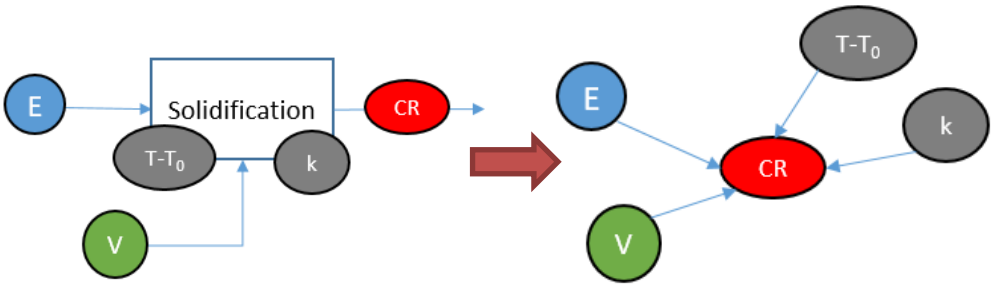

Figure 22. Presentation of functional model and causal graph for equation 13.

The modeling path 2 from the Figure 21 is used if no pre-existing knowledge is available. This is the case if no models or equations have been discovered by a state of the art search. In this case the first step is consisting to list the possible variables that can have an effect on the system. This latter approach can be though as the basic approach of DACM and it is presented in more detail in the previous chapter. A computer tool is currently under development to support this process. With that tool, it is possible to automatically generate causal graphs if an initial set of variables have been discovered and if those variables have been allocated to different functions pertaining to the function model of interest.

Both of the modeling paths can lead to qualitative simulation where contradictions can be discovered. A contradiction in a causal network is a node where contradictory objectives are simultaneously present. Those objectives are variables that should be simultaneously maximized and minimized. The discovery of a contradiction is a sign of a weakness. The traditional answer to this problem is to propose a tradeoff between the two objectives. In the TRIZ approach [64] the goal is to remove those contradictions by proposing inventive principles that can modify the causal graph or the colors associated with the variables in the causal graph.

Another usage of the causal graph and its associated equations is to make quantitative simulations. This can be done by transforming the model into a system dynamic model and implementing it into a system dynamic software tool such as Vensim or Stella. This has not implemented yet to the work and it is surely a future development for this research work.

The main objective of this thesis can be divided into five goals. First the innovative modeling approach is presented. Second, the way DACM work and how it can be used in support of designing and organizing experiments. Third objective is the validation of the model created via the support of design of experiment and its analysis method. Fourth goal is in to create a simulator for DED processes from the model. Last goal but not least is to connect the behavior of the machine and the properties of the manufactured part in a single integrated model.

CMT-process uses the energy of the produced arc to melt a filler material. The material is deposited on a substrate. From the tip of the wire where the molten droplets are created. Simultaneously, the movement of the nozzle creates layer by layer the desired shape, in this case a weld bead. There are several characteristic of interest in the CMT process and in the production of that bead, they are summarized in Figure 23.

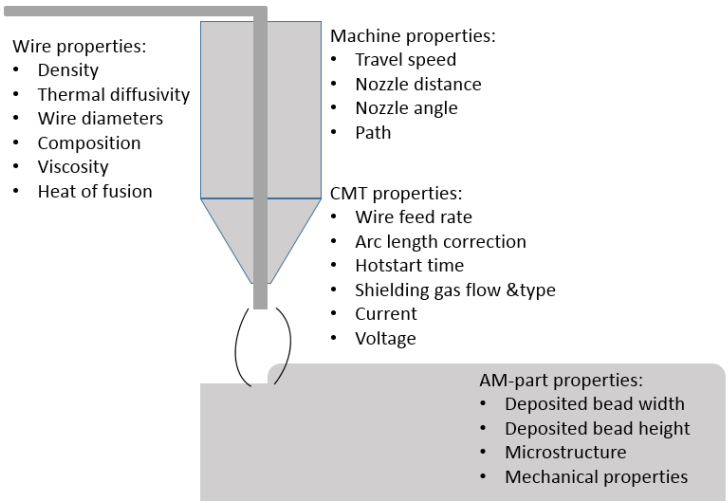

Figure 23. Parameters and variables in CMT additive manufacturing.

In CMT the arc melts the filler material creating a melt droplet at the tip of the wire this molten droplet is transferred to substrate material. Attaching these droplets together creates a bead and together with the simultaneous movement of the nozzle, multiples beads are created that form the final part. For simplicity in this model droplet are thought as a continuous feed, since of the whole deposition process takes place in order of magnitude of few milliseconds. Gathering knowledge about the bead properties and the effect of parameters on the shape and quality are both important aspects to consider. Therefore, the first model created is for a model of a single bead. In the Figure 24, the architecture of the process is described.

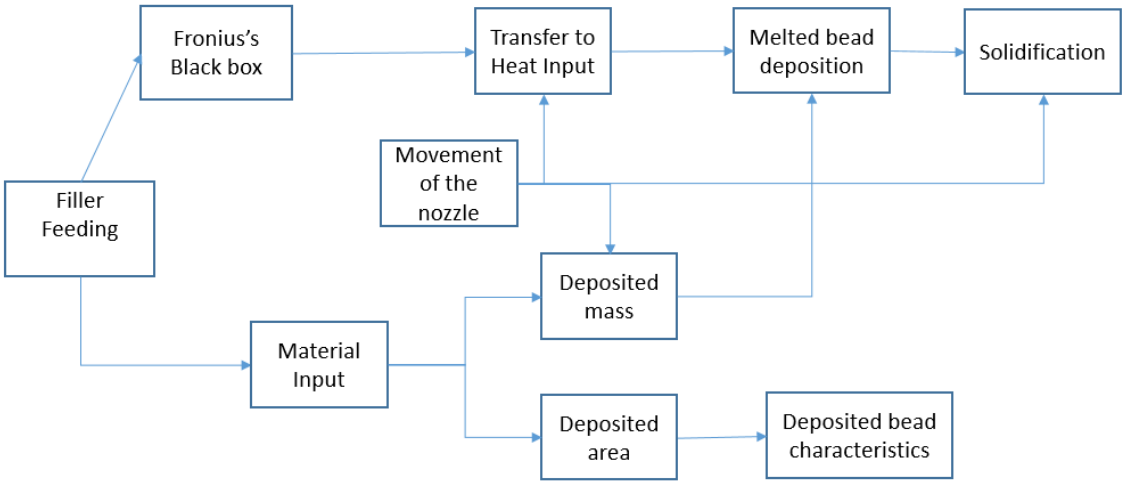

Figure 24. Presentation of the CMT system.

In the Table 9, the variables affecting the system properties are listed. They are the result of an analysis with specialists. Their symbols, unit and dimensions are also listed. Colors for each variable is provided in the table. Green color is selected for independent design variables, blue color is selected for dependent design variables, red color is selected for design variables that are used to assess the global quality of the desired performances. Black is a color selected for variables that are imposed by the environment of the system. The choice of those colors highlight the objectives and design perspectives underlying the creation of the model. A part of the analytical process can consist of changing those colors to test different alternative viewpoints. The model created in this work aims at predicting the cooling time and the bead size. Those parameters are selected as red in the model.

Table 9. System variables and their unit and dimensions.

Parameters	Symbol	Unit	Dimension	
Arc length correction	ALC	%		Independent
Dynamic correction	DC	%		Independent
Average current	I_{ave}	Ampere	A	Dependent
Average voltage	U_{ave}	Volt	$ML^2T^{-3}A^{-1}$	Dependent
Energy	P	Watt	ML^2T^{-3}	Dependent

Heat input	E	J/m	LMT^{-2}	Dependent
Wire feed rate	WRF	m/s	LT^{-1}	Independent
Volume feed rate	VFR	mm^3/s	M^3T^{-1}	Dependent
Mass	M	g	M	Dependent
Nozzle travel velocity	V	m/s	LT^{-1}	Independent
Thermal diffusivity	α	α=k/(ρ*Cp)	L^2T^{-1}	Exogenous
Density	ρ	kg/m^3	ML^{-3}	Exogenous
Thermal conductivity	k	W/(m*K)	$MLT^{-3}t^{-1}$	Exogenous
Specific Heat Capacity	C_p	joule/°C	$L^2T^{-2}t^{-1}$	Exogenous
Viscosity	μ	Pa*s	$ML^{-1}T^{-1}$	Exogenous
Melting point	T_m	°C	t	Exogenous
Heat of fusion	h_f	Joule/g	L^2T^{-2}	Exogenous
Shielding gas flow rate	GR	m^3/s		Exogenous
Filler diameter	d	m	L	Dependent
Bead width	W	m	L	Performance
Bead height	Z	m	L	Performance
Solidification time	T_f	s	T	Performance
Machine efficiency	ŋ	-	-	Exogenous
Temperature difference	$T-T_0$	°C	t	Exogenous

This model has been created with several methods, functional presentation of the model is in Figure 25. Firstly, to fully understand the Fronius machine, a reverse engineering model of the parameters was created. Two separate theoretical inputs where used for heat input and solidification. The modelling path 1 was used. Additional parts in the model where added using the modelling path 2.. This is summarized in the figure below.

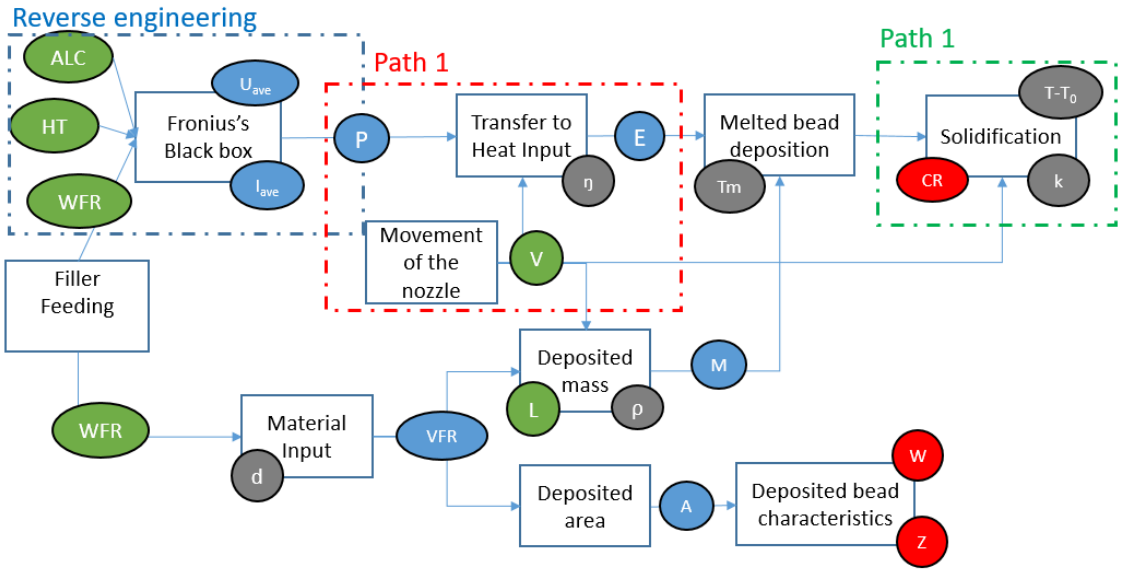

Figure 25. Functional presentation of CMT process with system variables.

From this functional model and the allocation of variables to the model, a causal graph was created using both automated causality rules for the modelling path 2 and representation of the equations for heat input and solidification for path 1. The resulting graph is presented in Figure 26.

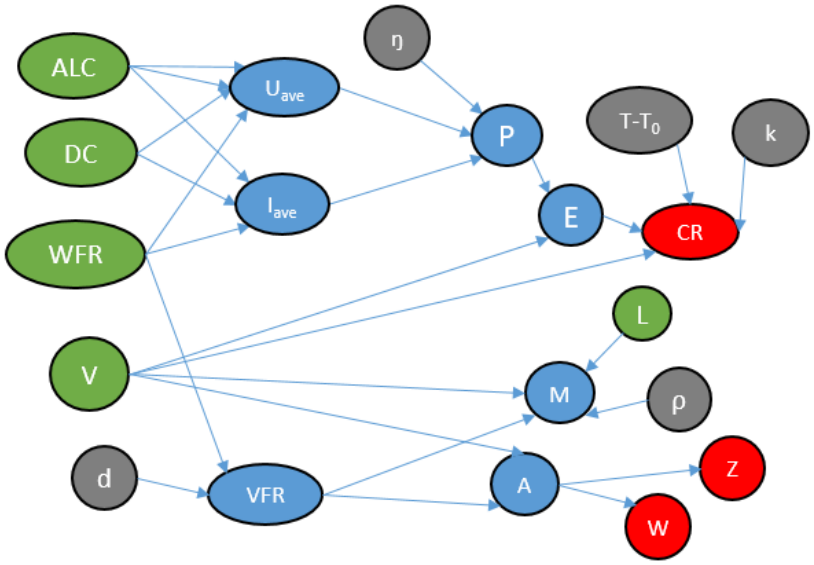

Figure 26. Causal graph for bead width, height and solification time.

6.3.1 Reverse engineering of a part of the CMT parameters' model

Understanding the internal structure of an Additive Manufacturing process is often an issue for researchers but also for companies using the Additive Manufacturing equipment. In this Directed Energy Deposition technology and more specifically using the CMT technology, we are also facing similar difficulty. The internal parameters of the Fronius CMT control system is a black box to which we have little access. In order to achieve our goal of developing a precise model of the process, we need to understand the behavior of this black box and for that we are using our experimental protocol to reverse engineer this black-box. Below the process is described using our experiments.

CMT is controlled via four main controllable parameters, wire feed rate (WFR), velocity (V), arc length correction (ALC) and hot start time or dynamic correction (HT). The experiment was organized with the Taguchi approach. A Taguchi orthogonal array table L9 was selected using the degree of freedom computation from the Taguchi method and each factor was chosen by considering 3 levels. The three factors affecting the process in this black box are, the wire feed rate (WFR), arc length correction (ALC) and hot start time (HT). Also the velocity (V) was chosen as a one factor since it bring variety in the heat input and beam size. The number of levels were selected based on the expected linearity (2 levels) or non-linearity (3 levels) of the phenomena. The ratio between WFR and V was selected in order to produce continuous bead. This was done by initial tests. Unknown

parameters ALC and HT were selected to have three levels. The experiment table is presented in Table 10 and the magnitude of the levels. Experiment were conducted for two materials (i.e. an aluminium alloy and a steel) to see if similar parameters have similar impacts or different impacts.

The green variables in the table below are the controlled variables. the red variables are the variables measured via the experiments. They are representing the performance variables of interest to populate and compute our model. In these experiments the parameters affect were power, P, current, I, voltage, U, heat input, E, area of the bead, A, secondary dendrite arm spacing, SDAS and local solidification time, ST, was examined.

Table 10. Orthogonal array for the design of experiments.

	WFR [m/min]	V [mm/s]	ALC [%]	HT [%]	U [V]	I [A]	P [W]	E [J/m]	A [mm^2]	SDAS
1	3,5	5	-30	-5						
2	3,5	10	0	0						
3	3,5	15	+30	+5						
4	5,5	5	0	+5						
5	5,5	10	+30	-5						
6	5,5	15	-30	0						
7	7,5	5	+30	0						
8	7,5	10	-30	+5						
9	7,5	15	0	-5						

6.3.2 Validation

This model was validated in several phases. Firstly, the area, A, and mass, M, were examined, the causal graph for only this phase is presented in Figure 27. Green variables in the model presented in this figure are the control parameters. L the length of the bead was kept constant because it was hypothesized that it had no importance on the value of the objective variables. All other variables in black were not included in this experimental protocol and were maintained constant to avoid generating noise. Those variables were fixed and considered exogenous despite the impact they have almost certainly on the mass deposited (M) and the area of the bead (A). It was hypothesized that to get a smaller M and A we need a smaller d and ρ. In a first glance, it was considered sufficient. the focus was given to the Wire feed rate impact (WFR) and the velocity of the welding (V). In the figure below, the performance variables are in red. They are the mass (M) and area (A) of the bead. The Length (L) of the bead was kept constant at a value of 50 mm. Each test set was run four time to integrate the variation.

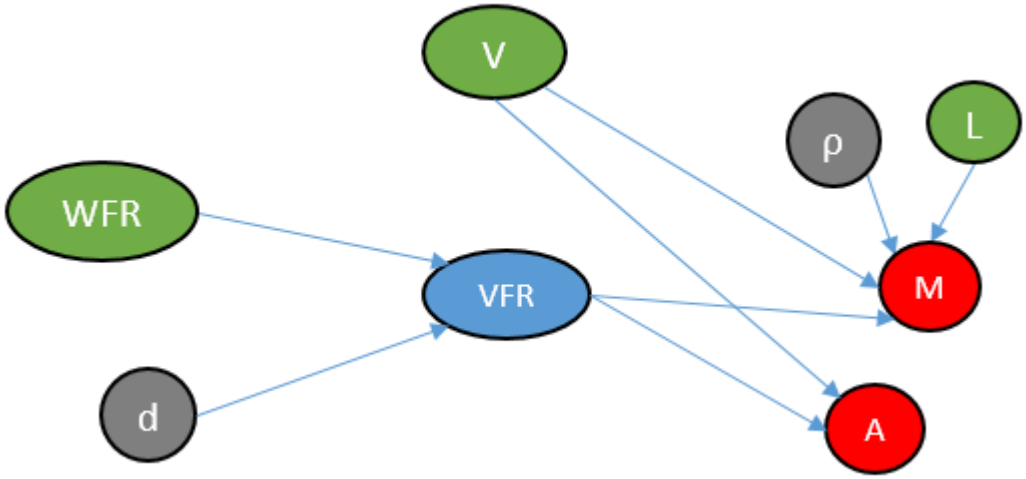

Figure 27. Causal graph for area and mass.

Table 11. Test plan for evaluating area and mass.

	V [mm/s]	WFR [m/min]
1	6	5
2	6	5
3	6	5
4	6	5
5	10	5
6	10	5
7	10	5
8	10	5
9	13	5
10	13	5
11	13	5
12	13	5

7. RESULTS

In this chapter results for the experiments are presented and analyzed. First the analysis of the experiments to understand the CMT parameters for AlSi5 and AISI 316L stainless steels is presented then results for the material evaluation of the AlSi5. Then the validation of the created model and short presentation of the results when this process was used as an additive manner.

7.1 Results of reverse engineering for CMT parameters for AlSi5

CMT-parameters were studied via the Taguchi's orthogonal array L9, shown in Table 12 with the measured experiments. In these experiments the parameters affect were power, P, current, I, voltage, U, heat input, E, area of the bead, A, secondary dendrite arm spacing, SDAS and local solidification time, ST, was examined. The results were analyzed by ANOVA. Figure 28 presents the summarized results for aluminum.

Table 12. Results for reverse engineering experiments for AlSi5.

	WFR [m/min]	V [mm/s]	ALC [%]	HT [%]	U [V]	I [A]	P [W]	E [J/m]	A [mm^2]	SDAS	ST
1	3,5	5	-30	-5	101	68	686,8	0,137	11,519	0,131977	$1{,}38\times10^{-05}$
2	3,5	10	0	0	12,1	72	871,2	0,0871	5,306	0,088813	$4{,}21\times10^{-06}$
3	3,5	15	+30	+5	17,4	76	1322,4	0,0882	3,777	0,062659	$1{,}48\times10^{-06}$
4	5,5	5	0	+5	18,8	92	1729,6	0,346	16,094	0,10218	$6{,}41\times10^{-06}$
5	5,5	10	+30	-5	18,8	127	2387,6	0,239	10,396	0,069723	$2{,}04\times10^{-06}$
6	5,5	15	-30	0	16,6	127	2108,2	0,141	4,684	0,069485	$2{,}02\times10^{-06}$
7	7,5	5	+30	0	19,4	150	2910	0,582	24,709	0,111238	$8{,}27\times10^{-06}$
8	7,5	10	-30	+5	19	91	1729	0,173	12,000	0,081079	$3{,}2\times10^{-06}$
9	7,5	15	0	-5	18,6	165	3069	0,205	10,685	0,077177	$2{,}76\times10^{-06}$

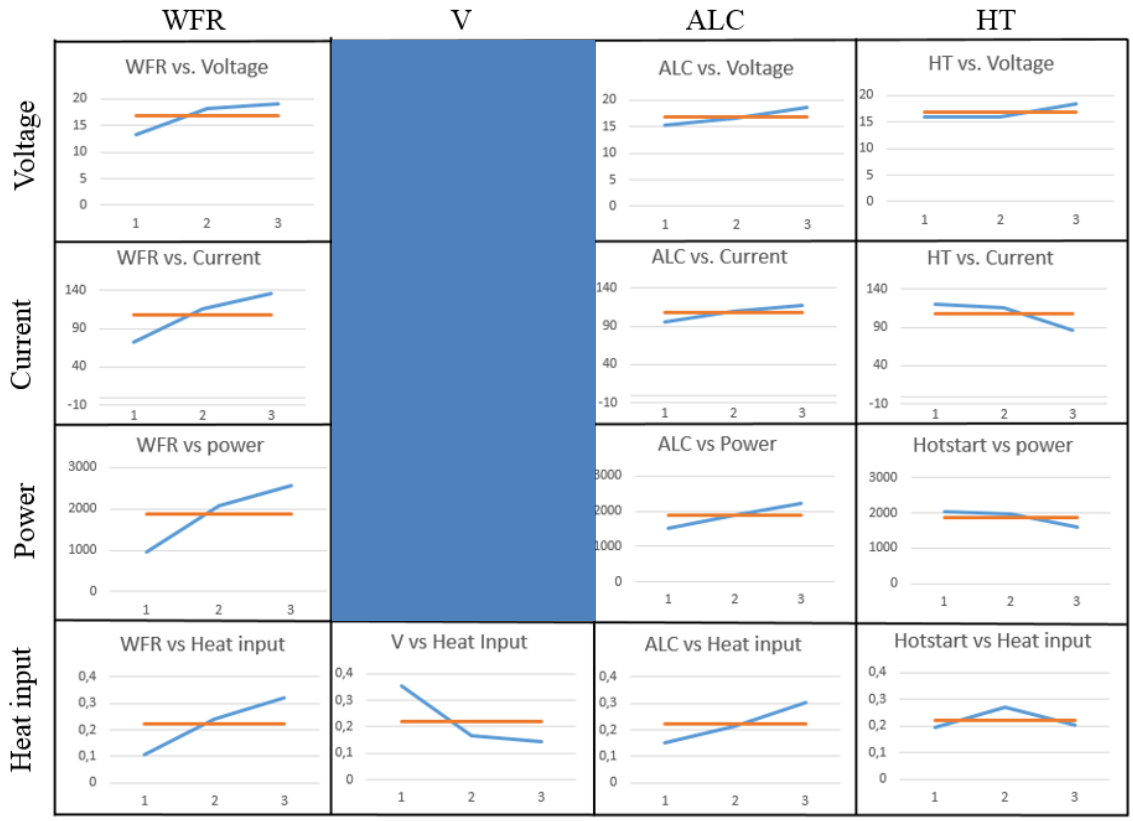

Figure 28. ANOVA-results for the alloy AlSi5.

The material rate should increase with the WFR, since more material is introduced to the system. The more material you have the more energy is needed to melt the material effectively. The more energy is need to melt material the more heat is input to the system, although increasing travel speed gives less mass and therefore less heat input is needed. This is already known from theory. Also, the equation 2 can be exploited. WFR and velocity have two opposite effect on the heat input and mass and this is fulfilling the theory. The energy is effected by the current and voltage of the system, which are controlled by WFR, ALC and HT. And from the theory, by increasing HT should increase heat input, but this wasn't found in our tests. Increasing ALC decreases the WFR in the arc phase and therefore increases the energy. The arc acts more like long arc and more energy is needed to across the gap between filler and substrate.

Unknown parameters, ALC and HT effect is unknown and this reverse engineering tests purpose was to clarify those parameters and find equations determining current and voltage by regression for each variable. A basic nonlinear regression was run for the experiment results to determine current and voltage of the Fronius apparatus. From the ANOVA results presented in Figure 28 can be determined that WFR and ALC acts linearly and HT more exponentially. Equations for current and voltage are presented below.

$$I = 1{,}126973WFR + 0{,}369082ALC - 0{,}12814HT^2 \qquad (20)$$

$$U = 0{,}165383WFR + 0{,}054505ALC + 0{,}082653HT^2 \quad (21)$$

From the equations 20, 21 and 2 can be determined the heat input. The calculated and measured values for the experiment are presented in a Table 13.

Table 13. Calculations and measurements from the validation tests and error value.

Measured			Predictions			Error-%		
Current	Voltage	Heat input	Current	Voltage	Heat input	Current	Voltage	Heat input
68	10,1	0,13736	57,83367	10,07302	0,116512	14,95049	0,26716	15,1777
72	12,1	0,08712	65,70252	9,641844	0,063349	8,746502	20,31533	27,28496
76	17,4	0,08816	79,9786	13,34331	0,071145	-5,235	23,31433	19,29983
92	18,8	0,34592	106,5132	17,227	0,366981	-15,7752	8,367014	-6,08831
127	18,8	0,23876	117,5857	18,86215	0,221792	7,412847	-0,33057	7,106785
127	16,6	0,140547	92,23714	13,52554	0,08317	27,37233	18,52085	40,82359
150	19,4	0,582	151,9441	22,30805	0,677915	-1,29605	-14,99	-16,4803
91	19	0,1729	133,0028	21,10408	0,28069	-46,1569	-11,0741	-62,3425
165	18,6	0,2046	144,0752	22,73923	0,218411	12,68168	-22,2539	-6,75005

Results indicate that the prediction equations aren't working so efficiently. It is important to remember that the measured values are averages of the whole process from the start of the weld till the end. Current and voltage can change dramatically between

7.2 Results of reverse engineering for CMT parameters for AISI 316L-stainless steel

Similar tests were carried out with stainless steel, in order do determining differences with the synergic lines. Test was carried with the same plan as with AlSi5. Results were analyzed by ANOVA and they are presented in Figure 29. ANOVA-results for steel. When comparing the results with AlSi5 can some differences be found. For AlSi5 the current and voltage travelled in a larger range, maximum for current was just below 140 A and voltage just below 20 V. For steel maximum were 125 A and 17 V, respectively. This can be explained by the higher melting temperature of aluminums oxides.

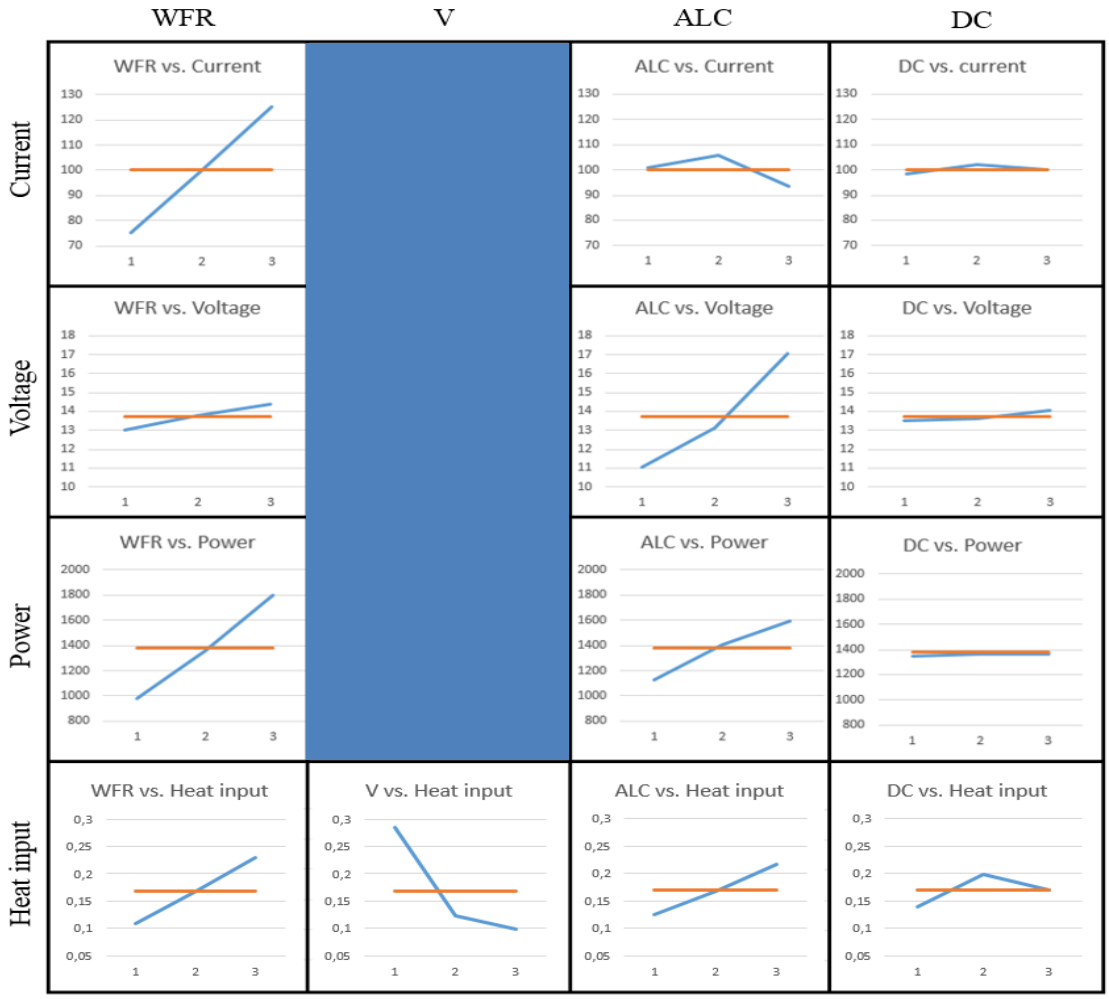

Figure 29. ANOVA-results for steel.

Other great difference is that ALC seems differ highly with voltage, increase as well with it did with AlSi5 but more drastically. Dynamic correction, DC, didn't seem to have an influence. Otherwise it acts similar as in AlSi5.

A same basic nonlinear regression was run for the experiment results to determine current and voltage of the Fronius apparatus. Equations derived from the regression are presented below.

$$I = 1{,}054748WFR + 0 \times ALC + 0{,}177287DC^2 \quad (22)$$

$$U = 0{,}126062WFR + 0{,}078434ALC + 0{,}083535DC^2 \quad (23)$$

Comparing the result to the results gained from aluminium alloy equations do act similarly. Although, current has several differences, such as ALC has a coefficient of zero and the sign for DC is positive when for HT it was negative. Full calculations are expressed in Table 14. Like with aluminium the error has large variation and the predictions cannot be reliable.

Table 14. Calculations and measurements for the validation tests and the error value.

Measured			Predictions			Error-%		
Current	Voltage	Heat input	Current	Voltage	Heat input	Current	Voltage	Heat input
75	10	0,15	65,92396	7,084785	0,093411	-12,1014	-29,1521	-37,7257
76	12	0,0912	61,49179	7,34943	0,045193	-19,0897	-38,7548	-50,4463
75	17,1	0,0855	65,92396	11,79081	0,05182	-12,1014	-31,0479	-39,3921
106	13,4	0,28408	101,1209	13,64449	0,275949	-4,60293	1,824587	-2,86233
84	16,6	0,13944	101,1209	15,99751	0,161768	20,38202	-3,62948	16,01278
109	11,4	0,08284	96,68872	9,203115	0,059322	-11,2947	-19,2709	-28,3891
121	17,5	0,4235	131,8435	18,11079	0,477558	8,96154	3,490251	12,76457
119	11,7	0,13923	136,2756	15,49314	0,211134	14,51734	32,41998	51,64384
136	13,9	0,126027	136,2756	17,84615	0,162133	0,202673	28,38957	28,64978

7.2.1 Results of material characterisation

Process parameters effects on the bead characteristic was also examined. CMT-process parameters, ALC and HT, have only minor effect on the size. When velocity increases size decreases and when wire feed rate increases the size increases as well. It is a must to point out that with AlSi5 not all beads were continuous, first three beads suffered lack of heat or material and therefore are insufficient when though final quality.

Microstructure and hardness test were analyzed for the samples from clarification test. Microstructural changes are presented in Figure 30. From the figures, already can be declared that the dendrite size decreases with velocity of the nozzle.

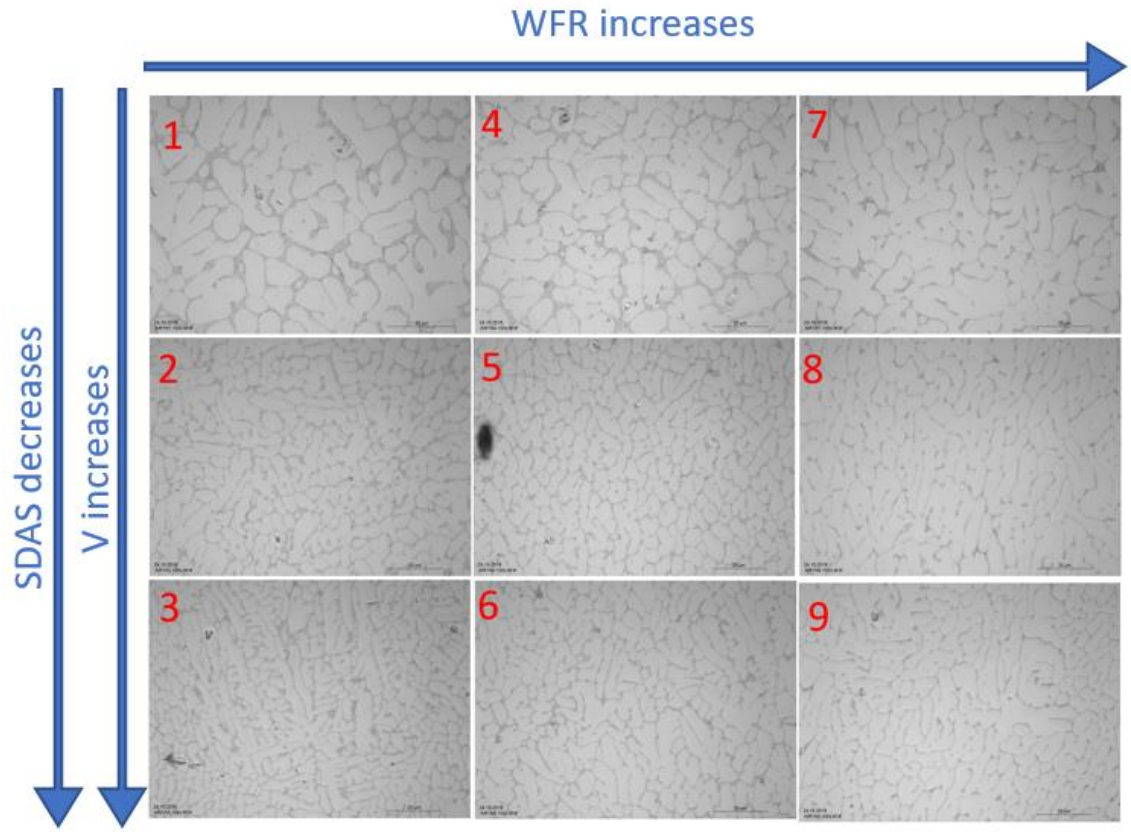

Figure 30. Microstructural evaluation of samples in clarification tests for AlSi5.

From the figures, secondary arm spacing was determined. Results are presented in Table 12, and verifies the figure analyze. Dendrite spacing decreases with increasing velocity of the nozzle. In Figure 31 is visualized the results, how the heat input effects the solidification time. The more heat is inputted the more bead has time to solidify and therefore larger dendrite forms. Heat input is one of the important variables when examining microstructure and solidification.

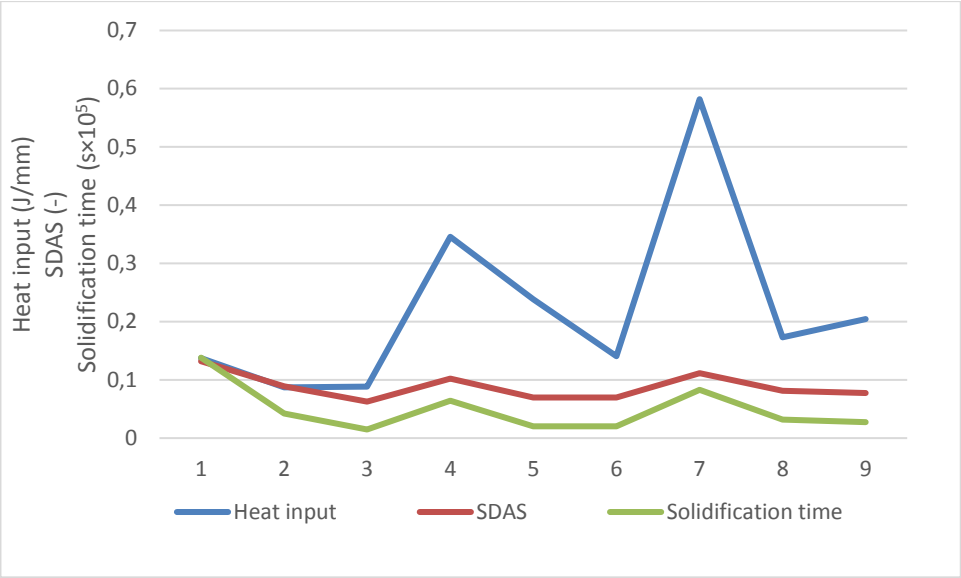

Figure 31. Visualization of heat input, SDAS and solidification time in different samples.

Every sample had also surface hardness test. The results with sample numbers is presented below in Figure 32. Upper point of the bead had the lowest hardness throughout the test period, expect in bead number 7. Also, beads 1,2 and 3 had significantly higher harness in the base area.

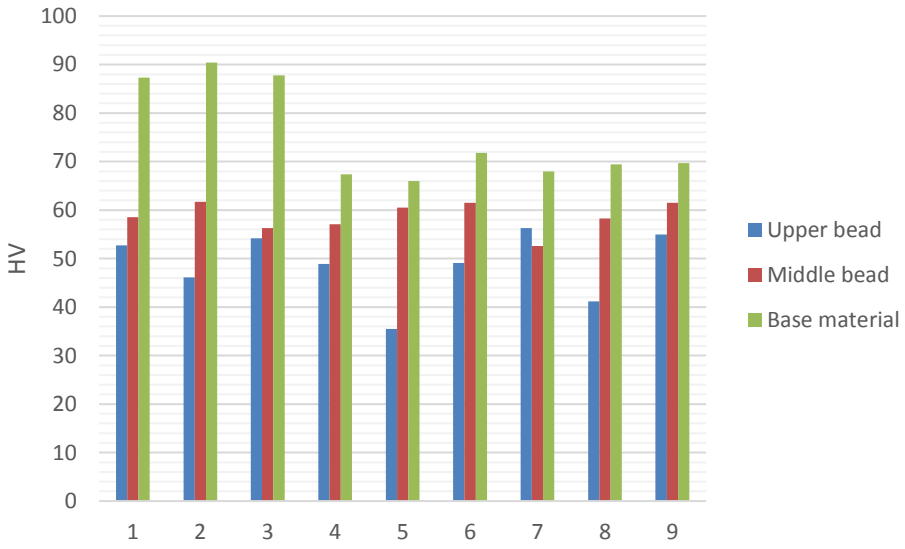

Figure 32. Hardness measurements results

7.3 Validation of the model

The validation of the model was conducted for mass and area of the bead. Substrate material was weighed after every bead and then calculated the value of single bead. Area

was measured from the cross section of the bead. Samples were cut and with photo application the area of the cross section was measured.

Dimensionless groups were computed for each causal relation. A simple linear algebra transformations were used to compute behavioral laws of the variables.

$$I_{ave} = f(ALC, HT, WFR) \tag{24}$$

$$U_{ave} = f(ALC, HT, WFR) \tag{25}$$

$$VFR = f(WFR, d) \tag{26}$$

$$A = f(V, VFR) \tag{27}$$

$$M = f(V, VFR, L, \rho) \tag{28}$$

$$P = f(I_{ave}, U_{ave}, \eta) \tag{29}$$

$$E = f(P, V) \tag{30}$$

$$CR = f(E, V, T - T_0, k) \tag{31}$$

In this thesis few variables have been already determined by the reverse engineering or from theory. Equations for VFR, M and A needs to be determined. An example table of the process is presented in Table 15. Number in the table present the amount of certain dimension the variable has, for example in this case volume feed rate (VFR) is acting as a target variable and has dimensions of mm^3/s, which means length is 3 and the time is -1 and so on. Other variables, WFR and d, are cause variables.

Table 15. Dimensional analysis for volume feed rate.

	[B]	[A]	
∏VFR	VFR	WFR	d
Length	3	1	1
Time	-1	-1	0

With the equation 32 can be the desired exponents for each variable be determined.

$$[C] = ([A]^{-1} \times [B])^T \tag{32}$$

From this the exponents for all needed variables are presented below.

$$\pi_{VFR} = WFR \quad \times d^2 \tag{33}$$

$$\pi_M = V^{-1} \times VFR \quad \times L \quad \times \rho \tag{34}$$

$$\pi_A = V^{-1} \times VFR \quad (35)$$

Results are presented below in Table 16. Predicted values of M and A were calculated by using equations 34 and 35.

Table 16. Results for evaluation of area and mass.

V [mm/s]	Measured M [g]	Measured A [mm^2]	Predicted M [g]	Predicted A [mm^2]	%-error M	%-error A
6	2,325	17,0285	2,85	19,92	18,42	14,52
10	1,5025	9,24525	1,71	11,95	12,13	22,63
13	1,215	6,353	1,32	9,194	7,95	30,90

Result indicate that the model is predicting area and mass to the same decimal point and quite close to the measured value. Even though so far, the model has not concerned any thermal input. Thermal input and its effects for example viscosity and density of the material changes with the temperature and therefore can affect the final structure. Error other hand show that it area is in acceptable and as the velocity of the nozzle increases the error increases in the mass values and decreases in area values. Since the area can vary quite a lot depending where it was measured more cross section samples for sample test run 1 and 2 was measure in order to see the variation.

7.4 Multiple bead samples

Multiple bead was produced vie CMT apparatus. Hardness profile throughout the sample was created and microstructure was examined. For AlSi5 hardness profile is presented in Figure 33. No great differences can be found through the sample, other than the hardness increased towards the root of the wall.

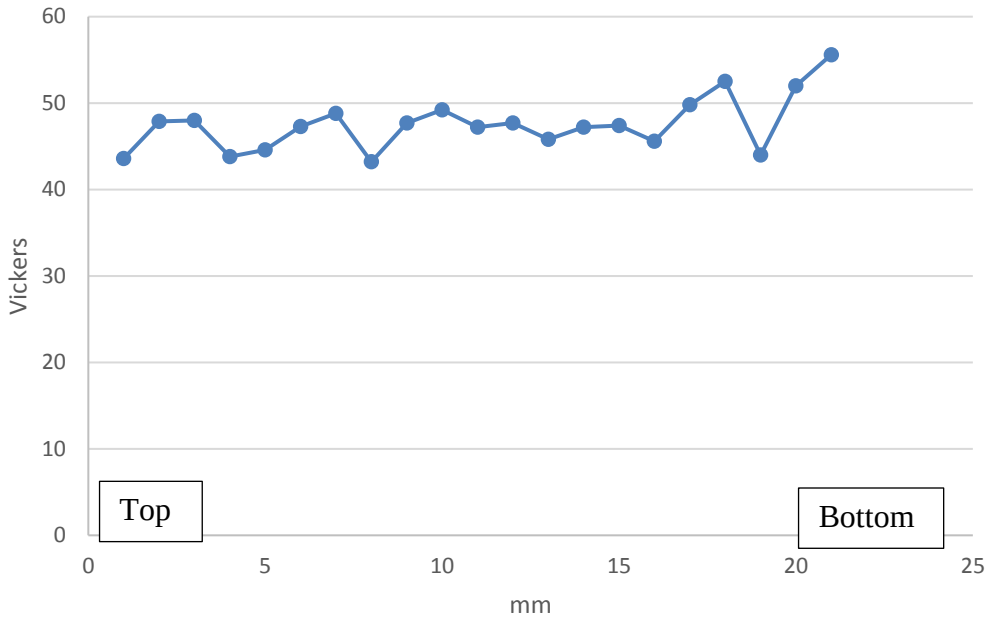

Figure 33. Hardness profile of multiple bead deposit of AlSi5.

Microstructure of the bead is presented in Figure 34. There can clearly see a difference in dendrite size, when moving close to bottom of the weld, this might be since conduction rate is higher at the bottom of the deposit or that the thermal cycle have increased the time to solidify and therefore the dendrite size is larger.

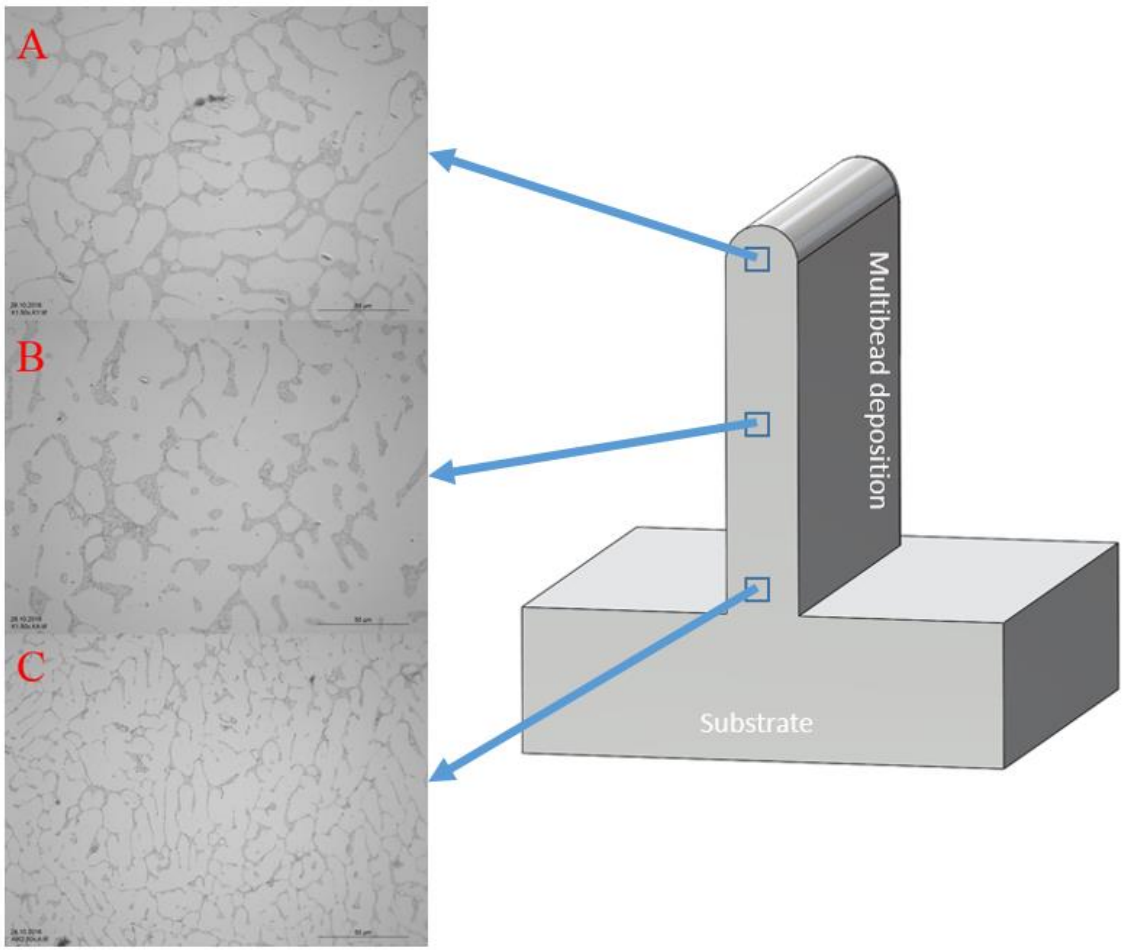

Figure 34. Microstructure examination from the wall.

8. DISCUSSION

CMT is a rather new and complex welding method that has gained interest in additive manufacturing community. In this thesis one of the goals was to examine the CMT process and the parameters of the process. Prakasham et al.[24] stated that CMT is a highly controlled process. Weld quality is mainly gained by controlling wire feed speed and travel velocity. Fine tuning is achieved with CMT's synergic lines. According to the result of this article, wire feed rate had the most influence on process parameters such as voltage and current. In his doctoral thesis, Sequeira Almeida [26] reported similar results. Wire feed rate increases average current and voltage in a positive manner as well as the average power of the system.

Main parameters that affected the size of the bead were velocity and wire feed rate. Other parameters that could have an effect on the bead size were not studied here. Such parameters could be for example nozzle angle and stick-out-of-the-wire. Increase in travel velocity results in a smaller bead size. This is because less material is deposited into the same unit of length. However, when increasing the wire feed rate also the bead size increases, i.e. more material is deposited into the same unit of length.

Metallurgical evaluation of single beads was carried out to see how the process parameters such as travel velocity and wire feed rate affect the solidification time and therefore the microstructure. Results showed that the structure is coarser when velocity is decreased. The finding is supported by theory, since lower velocity results in higher local heat input and thus longer cooling time of the material. Zhang et al. [16] studied the parameter effect on magnesium clads and found similar results. They also stated that when solidification time is high the material is less likely to have porosity. The pores have more time to escape from the structure. In these samples, no significant porosity was found.

Hardness test were carried for each sample, the results were inconclusive and any relationships cannot be drawn from them. First three beads base material had significantly higher hardness than the rest of the beads. This can be result from the fact that there wasn't enough heat or material to deposit continuous beads. This can resolve why the hardness hadn't drop in the first beads. Ding et al. [13] studied also tried to find relationships between process parameters and material properties, and found a slight effect of velocity on the hardness, but stated that the final hardness was mainly effected by the post treatment temperature.

Creating a model for additive manufacturing has raised interest. Firstly, a single bead must be modeled in order to understand the basic phenomena and subsequently the whole process. Single beads have been modelled quite a lot in welding and in coating technologies. Most approaches have been mathematical or thermal but also other options exist.

Our model was created using DACM primarily to predict the area and the mass of the bead. The accuracy of the predictions created with the model were fairly high but included some variance. The model did not include at the moment thermal input which is most probably a major of cause inaccuracy. This would be due to the changes in the cross-section area caused by difference in viscosity.

9. CONCLUSIONS

In this thesis, the goal was to examine rather new welding method called cold metal transfer and its possibility to use is as an additive manufacturing technique. The process itself is closed system and only some parameters can be adjusted by the user. In this thesis determining parameters that effect bead quality and some material characteristics were determined. And in last a model by using dimensional analysis conceptual modeling was created to predict quality and characteristics. This model was validated by several tests designed by the Taguchi method and the orthogonal array and ANOVA.

CMT process has been a closed process and one of the test carried out in this thesis was to determined how the machine acts, so called reverse engineering process. The object of those test was to determine how synergic lines work and how they differ between materials. Results showed that they act similarly between materials but the magnitudes differ. This is caused by the material properties. Different materials need more heat to melt than others. Comparing aluminum and steel, aluminum had higher power, even though aluminum has lower melting point.

The causal graph has to be updated below to account for possible missing causal links that have been identified. These links are important to examine and should be a future aspect of our work. In Figure 35 red arrows represent the missing links. These include the link between heat input and viscosity, the link between viscosity and the width of the bead, the link between cooling rate and SDAS and lastly the link between mass and the cooling.

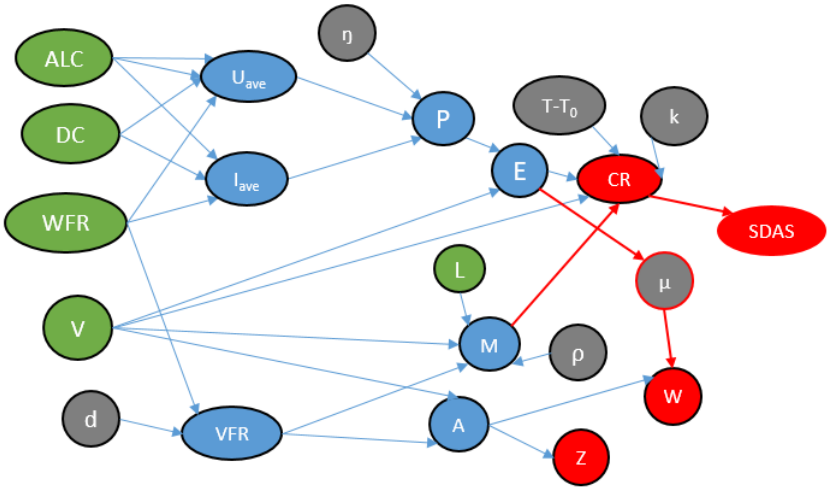

Figure 35. Updated causal graph for future work.

The logical next step is to implement the missing causal links into the model. Developing the model to predict the microstructures of multiple beads can also be a future target. Quantitative simulation should be run for this model and a simulator should be developed for DED-processes. Also, more parameters such as nozzle direction, stick out, would be beneficial to examine.

REFERENCES

[1] P. Srinivasa, O. P. Gupta, S. S. N. Murty, and A. B. Koteswara Rao, "Effect of process parameters and mathematical model for the prediction of bead geometry in pulsed GMA welding," *Int. J. Adv. Manuf. Technol.*, vol. 45, pp. 496–505, 2009.

[2] J. L. Mattsson, "Simplifications of Simulations in Additive Manufacturing," Luleå University of Technology, 2015.

[3] E. Coatanéa, R. Roca, H. Mokhtarian, F. Mokammel, and K. Ikkala, "A conceptual modeling and simulation framework for system design," *Comput. Sci. Eng.*, 2016.

[4] H. Mokhtarian, E. Coatanéa, H. Paris, T. Ritola, A. Ellman, J. Vihinen, K. Koskinen, and K. Ikkala, "A network based modelling approach using the dimensional analysis conceptual modeling (DACM) framework for additive manufacturing technologies," in *ASME 2016 International Design Engineering Technical Conferences and Computes and Information in Engineering Conference*, 2016.

[5] Y. S. Tarng and W. H. Yang, "Optimisation of the weld bead geometry in gas tungsten arc welding by the taquchi method," *Int. J. Adv. Manuf. Technol.*, vol. 14, pp. 549–554, 1998.

[6] "Standard Terminology for Additive Manufacturing Technologies." [Online]. Available: http://www.astm.org/FULL_TEXT/F2792/HTML/F2792.htm. [Accessed: 01-Jun-2016].

[7] W. E. Frazier, "Metal additive manufacturing a review," *J. Mater. Eng. Perform.*, vol. 23, no. 6, pp. 1917–1928, 2014.

[8] P. a Kobryn, N. R. Ontko, P. L. P., and T. J. S., "Additive Manufacturing of Aerospace Alloys for Aircraft Structures," *AVT-139 Spec. Meet. Amsterdam*, vol. May, no. 2006, 2006.

[9] B. Vayre, F. Vignat, and F. Villeneuve, "Metallic additive manufacturing: State-of-the-art review and prospects," *Mech. Ind.*, 2012.

[10] W. J. Sames, F. A. List, S. Pannala, R. R. Dehoff, and S. S. Babu, "The metallurgy and processing science of metal additive manufacturing," *Int. Mater. Rev.*, vol. 6608, no. March, pp. 1–46, 2016.

[11] W. E. Frazier, "Metal Additive Manufacturing: A Review."

[12] Y. K. Bandari, S. W. Williams, J. Ding, and F. Martina, "ADDITIVE MANUFACTURE OF LARGE STRUCTURES: ROBOTIC OR CNC SYSTEMS?"

[13] D. Ding, Z. Pan, D. Cuiuri, and H. Li, "Wire-feed additive manufacturing of metal components technologies, developments and future interests," *Int. J. Adv. Manuf.*

Technol., vol. 81, pp. 465–481, 2015.

[14] Metal additive manufacturing, "Applications for Additive Manufacture technology." [Online]. Available: http://www.metal-am.com/introduction_to_metal-additive_manufacturing/Applications. [Accessed: 10-Mar-2016].

[15] P. M. Sequeira Almeida and S. Williams, "Innovative process model of Ti-6Al-4V additive layer manufacturing using cold metal transfer (CMT)," in *21st Annual International Solid Freeform Fabrication Symposium*, 2010.

[16] H. Zhang, S. Hu, Z. Wang, and Y. Liang, "The effect of welding speed on microstructures of cold metal transfer deposited AZ31 magnesium alloy clad," *Mater. Des.*, vol. 86, pp. 894–901, Dec. 2015.

[17] G. Posch, F. Kalchgruber, H. Hackl, and H. Chladil, "Manufacturing of turbine blades by shape giving CMT-welding," in *Metal Additive Manufacturing Conference*, 2014.

[18] Fronius, "Cold Metal Transfer/The technology," Feb. 2014.

[19] B. Mezrag, F. Deschaux-Beaume, and M. Benachour, "Control of mass and heat transfer for steel/aluminium joining using Cold Metal Transfer process," vol. 20, no. 3, pp. 189–198, 2015.

[20] J. Lukkari, *Hitsaustekniikka*, First Edit. Helsinki: Opetushallitus, 1997.

[21] T. P. Hasselberg, "A Feasibility Study of 'Cold Metal Transfer' – Gas Metal Arc Welding," Rensselaer Polytechnic Institute, 2009.

[22] P. Kazanas, P. Deherkar, P. M. Sequeira Almeida, H. Lockett, and S. W. Williams, "Fabrication of geometrical features using wire and arc additive manufacture," *J. Eng. Manuf.*, vol. 226, no. 6, pp. 1042–1051, 2012.

[23] Fronius International GmbH, "CMT Process," 2013.

[24] G. Prakasham, L. S. R. Krishna, and A. S. Kumar, "A Review on the Effect of Various Process Parameters in Cold Metal Transfer (CMT) GMAW Welding," vol. 5013, no. 5, pp. 432–435, 2016.

[25] M. Willinger, "MIG / MAG CMT & CMT Adv. Parameter Adjustments," 2014.

[26] P. M. Sequeira Almeida, "Process control and development in wire and arc additive manufacturing," Cranfield University, 2012.

[27] B. Cong, J. Ding, and S. Williams, "Effect of arc mode in cold metal transfer process on porosity of additively manufactured Al-6.3%Cu alloy," *Int. J. Adv. Manufactruing Technol.*, vol. 76, pp. 1593–1606, 2015.

[28] P. Wang, S. Hu, J. Shen, Y. Liang, and J. Pang, "Effects of electrode positive/negative ratio on microstructure and mechanical properties of Mg/Al dissimilar variable polarity cold metal transfer welded joints," *Mater. Sci. Eng. A*,

vol. 652, pp. 127–135, Jan. 2016.

[29] S. Kou, *Welding Metallurgy*, Second Edi., vol. 822, no. 1–3. New Jersey: John Wiley & Sons, 2003.

[30] N. Pépe, S. Egerland, P. A. Colegrove, D. Yapp, A. Leonhartsberger, and A. Scotti, "Measuring the Process Efficiency of Controlled Gas Metal Arc Welding Processes," *Sci. Technol. Weld. Join.*, vol. 16, no. 5, pp. 412–417, 2011.

[31] D. Porter, K. Easterling, and M. Sherif, *Phase transformations in metals and alloys*. Taylor & Francis Group, 2009.

[32] A. A. Antonysamy, "Microstructure, texture and mechanical property evolution during additive manufacturing of Ti-6Al-4V alloy for aerospace applications," University of Manchester, 2012.

[33] V. Lindroos, M. Sulonen, and M. Veistinen, *Uudistettu Miekk-ojan metallioppi*. Helsinki: Otava, 1986.

[34] D. H. Herring, "Grain size and its influence on material properties," *Ind. Heat.*, vol. August, 2005.

[35] T. W. Daniels, "Applicability of Cold Metal Transfer for Repair of," 2015.

[36] L. F. Lancaster, *Metallurgy of welding*, 6th ed. Woodhead Publishing, 1999.

[37] M. Ashby, H. Shercliff, and D. Cebon, *Materials engineering, science, processing and design*, First edit. Elsevier Ltd., 2007.

[38] Z. Wang, T. A. Palmer, and A. M. Beese, "Effect of processing parameters on microstructure and tensile properties of austenitic stainless steel 304L made by directed energy deposition additive manufacturing," *Acta Mater.*, vol. 110, pp. 226–235, May 2016.

[39] D. Herzog, V. Seyda, E. Wycisk, and C. Emmelmann, "Additive manufacturing of metals," *Acta Materialia*, vol. 117, pp. 371–392, 2016.

[40] N. Raghavan, R. Dehoff, S. Pannala, S. Simunovic, M. Kirka, J. Turner, N. Carlson, and S. S. Babu, "Numerical modeling of heat-transfer and the influence of process parameters on tailoring the grain morphology of IN718 in electron beam additive manufacturing," *Acta Mater.*, vol. 112, pp. 303–314, 2016.

[41] J. Gu, B. Cong, J. Ding, S. W. Williams, and Y. Zhai, "Wire+arc additive manufacturing of aluminium," in *Solid Freedom Fabrication Symposium*, 2014, pp. 451–458.

[42] C. Leinenbach, "Material Aspects in Metal Additive Manufacturing," Santa fe, 2015.

[43] W. Callister, *Materials science and engineering: An introduction*, 7th Editio. John Wiley & Sons, 2007.

[44] F. Wang, S. Williams, P. Colegrove, and A. A. Antonysamy, “Microstructure and Mechanical Properties of Wire and Arc Additive Manufactured Ti-6Al-4V.”

[45] T. Amine, J. W. Newkirk, and F. Liou, “Investigation of effect of process parameters on multilayer builds by direct metal deposition,” *Appl. Therm. Eng.*, vol. 73, no. 1, pp. 500–511, Dec. 2014.

[46] S. Bontha, N. W. Klingbeil, P. A. Kobryn, and H. L. Fraser, “Effects of process variables and size-scale on solidification microstructure in beam-based fabrication of bulky 3D structures,” *Mater. Sci. Eng. A*, vol. 513, pp. 311–318, 2009.

[47] X. Gong, J. Lydon, K. Cooper, and K. Chou, “Beam speed effects on Ti–6Al–4V microstructures in electron beam additive manufacturing.”

[48] R. M. Mahamood, E. T. Akinlabi, M. Shukla, and S. Pityana, “Scanning velocity influence on microstructure, microhardness and wear resistance performance of laser deposited Ti6Al4V/TiC composite,” *Mater. Des.*, vol. 50, pp. 656–666, 2013.

[49] J. D. Majumdar, A. Pinkerton, Z. Liu, I. Manna, and L. Li, “Microstructure characterisation and process optimization of laser assisted rapid fabrication of 316L stainless steel,” *Appl. Surf. Sci.*, vol. 247, no. 1, pp. 320–327, 2005.

[50] R. Bhaskar and A. Nigam, “Qualitative physics using dimensional analysis,” *Artif. Intell.*, vol. 45, no. 1–2, pp. 73–111, Sep. 1990.

[51] P. F. Mendez and F. Ordoñez, “Scaling Laws From Statistical Data and Dimensional Analysis,” *Trans. ASME*, vol. 72, no. September, pp. 648–657, 2005.

[52] R. K. Roy, *Design of Experiments Using The Taguchi Approach: 16 Steps to Product and Process Improvement*. John Wiley & Sons, 2001.

[53] S. Buyske and R. Trout, “Robust Design and Taguchi Methods,” *Design*, p. 6.

[54] S. Kumar, K. Scholar, P. Acme, and R. Sahai, “An Overview on Taguchi Method,” *Int. J. Eng. Math. Sci.*, vol. 1, no. 1, pp. 2319–4537, 2012.

[55] J. Antony, *Design of Experiments for Engineers and Scientists*. Elsevier, 2003.

[56] D. Khosrow, *Quality control, robust design and the Taguchi method*. Pacific Grove: Wadsworth & Brooks/Cole, 1989.

[57] D. C. Montomery, *Design and Analysis of Experience*, Fifth. John Wiley & Sons, 2001.

[58] Fronius, “CMT : Cold Metal Transfer A hot & cold process makes,” 2013.

[59] “Fronius International GmbH - Products - Arc welding.” [Online]. Available: http://www.fronius.com/cps/rde/xchg/SID-DD8681E9-936DDC2B/fronius_international/hs.xsl/79_6317_ENG_HTML.htm#.V8AHEnqXetQ.

[60] ABB Robotics, “Product specification IRB 4600,” 2014.

[61] ABB Robotics, “Product Specification IRBP/D2009,” 1914.

[62] AK Steel, “AK STEEL 316/316L STAINLESS STEEL DATA SHEET.”

[63] ASM, “Properties of Wrought Aluminum and Aluminum Alloys.” [Online]. Available: http://products.asminternational.org/hbk/do/navigate?navOn=true&src=/content/V06/D00/A01/index.htm. [Accessed: 08-Nov-2016].

[64] G. Altshuller, *Creativity as an exact science*. Luxembourg: Gordon & Breach, 1984.